Oncogenic KRAS suppresses store-operated Ca^{2+} entry and I_{CRAC} through ERK pathway-dependent remodelling of STIM expression in colorectal cancer cell lines.

Cristina Pierro[a,b], Xuexin Zhang[c], Cynthia Kankeu[a], Mohamed Trebak[c], Martin D. Bootman[b,d] and H. Llewelyn Roderick[a,b]*

[a]Laboratory of Experimental Cardiology, Department of Cardiovascular Sciences, KU Leuven, Leuven, Belgium

[b]Previously at Babraham Institute, Babraham Research Campus, Cambridge, UK

[c]Department of Cellular and Molecular Physiology and Penn State Hershey Cancer Institute, Penn State College of Medicine, Hershey PA 17033, United States.

[d]School of Life, Health and Chemical Sciences, The Open University, UK

*Address for correspondence: [a]Laboratory of Experimental Cardiology, Department of Cardiovascular Sciences, CDG 9th Floor, KU Leuven, Campus Gasthuisberg, Herestraat 49, B-3000 Leuven, Belgium

Tel: +3216377150

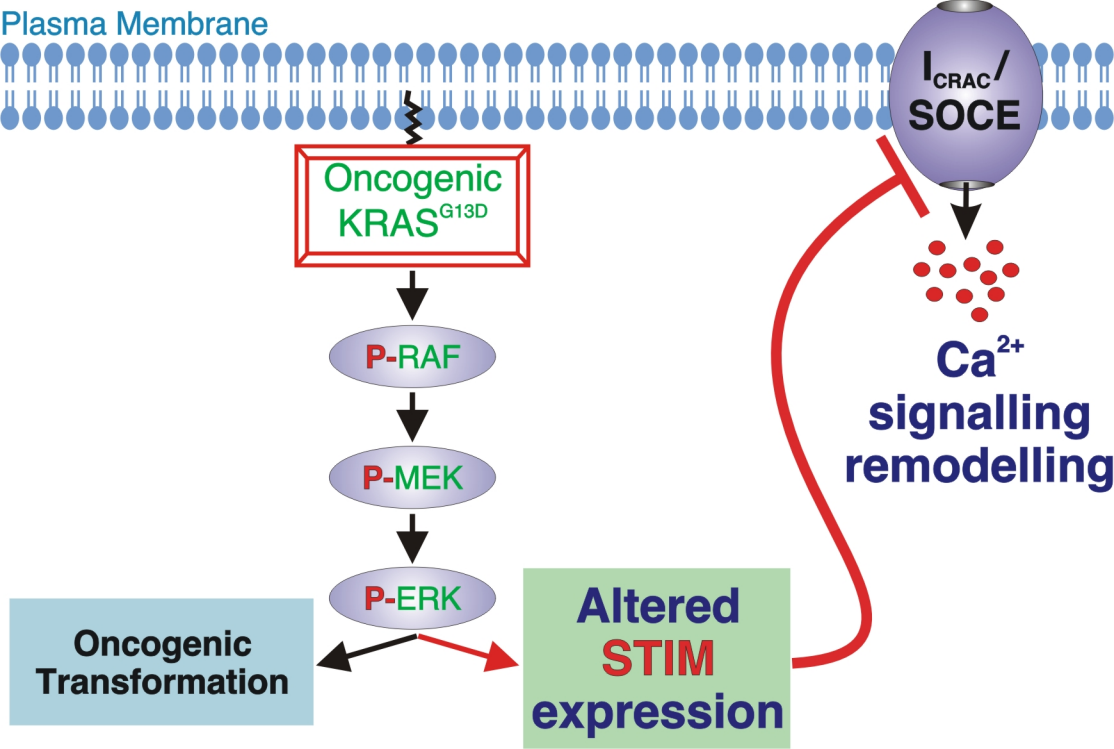
E-mail: llewelyn.roderick@kuleuven.be

Running title Oncogenic KRAS modulates SOCE via STIM expression in colorectal cancer

Keywords

Calcium signalling, STIM, KRAS, colorectal cancer cancer, ERK, SOCE/I_{CRAC}

Conflicts of Interest: None


Plasma Membrane
I_{CRAC}/ SOCE
Oncogenic KRAS^{G13D}
P-RAF
P-MEK
P-ERK
Ca^{2+} signalling remodelling
Oncogenic Transformation
Altered STIM expression

Abstract

The KRAS GTPase plays a fundamental role in transducing signals from plasma membrane growth factor receptors to downstream signalling pathways controlling cell proliferation, survival and migration. Activating *KRAS* mutations are found in 20% of all cancers and in up to 40% of colorectal cancers, where they contribute to dysregulation of cell processes underlying oncogenic transformation. Multiple KRAS-regulated cell functions are also influenced by changes in intracellular Ca^{2+} levels that are concurrently modified by receptor signalling pathways. Suppression of intracellular Ca^{2+} release mechanisms can confer a survival advantage in cancer cells, and changes in Ca^{2+} entry across the plasma membrane modulate cell migration and proliferation. However, inconsistent remodelling of Ca^{2+} influx and its signalling role has been reported in studies of transformed cells. To isolate the interaction between altered Ca^{2+} handling and mutated KRAS in colorectal cancer, we have previously employed isogenic cell line pairs, differing by the presence of an oncogenic *KRAS* allele (encoding $KRAS^{G13D}$), and have shown that reduced Ca^{2+} release from the ER and mitochondrial Ca^{2+} uptake contributes to the survival advantage conferred by oncogenic KRAS. Here we show in the same cell lines, that Store-Operated Ca^{2+} Entry (SOCE) and its underlying current, I_{CRAC} are under the influence of $KRAS^{G13D}$. Specifically, deletion of the oncogenic *KRAS* allele resulted in enhanced STIM1 expression and greater Ca^{2+} influx. Consistent with the role of KRAS in the activation of the ERK pathway, MEK inhibition in cells with $KRAS^{G13D}$ resulted in increased STIM1 expression. Further, ectopic expression of STIM1 in HCT 116 cells (which possess the KRASG13D mutation) rescued SOCE, demonstrating a fundamental role of STIM1 in suppression of Ca^{2+} entry downstream of $KRAS^{G13D}$. These results add to the knowledge of how ERK controls cancer cell physiology and highlight STIM1 as an important biomarker in cancerogenesis.

1. Introduction

The small GTPase RAS is a molecular switch that couples receptor tyrosine kinase (RTK) activation with downstream signalling pathways regulating cell proliferation, survival and migration. Somatic mutations at several levels in these pathways, for example in RTKs (EGFR), RAS itself, BRAF and PI3K, are highly prevalent in cancer and are responsible for the

constitutive activation of affected pathways observed [1]. Notably, underlining its importance in oncogenic transformation, *RAS* is mutated in 20-30 % of all cancers and up to 40% of colorectal cancer (CRC), which is the second and third most prevalent cancer in women and men, respectively, affecting over one million patients per year globally [2]. Of the three RAS isoforms, *KRAS* is most frequently mutated in cancer, and as the only essential isoform it has the greatest impact on cell biology [1]. The importance of growth factor signalling pathways in oncogenic transformation has placed them at the centre of cancer drug development efforts. To date however, while drugs targeting RTKs, BRAF, MEK and PI3K are at various stage of development or in use in the clinic, no effective drugs targeting KRAS are available [3].

Constitutive activation of KRAS in cancer is brought about through missense point mutations in the codons encoding Gly12, Gly13 or Gln61 [1]. Consequently, the activities of pathways downstream of KRAS are increased. KRAS signals via four main pathways: the RAF/MEK/ERK pathway, the PI3K/AKT pathway, the RAL pathway and the PLCε/PKC/Ca^{2+} pathway. These pathways do not act in isolation however but signal in concert. Notably, Ca^{2+} signalling pathways and the KRAS-RAF-MEK-ERK pathway interact at many levels [4,5]. For example, inhibition of BRAF increases the expression of Ca^{2+} ATPase isoform 4b (PMCA4) [6] and facilitates endoplasmic reticulum (ER)-mitochondrial Ca^{2+} transfer [7]. Upon phosphorylation, KRAS interferes with Bcl_{XL} interaction with and sensitisation of $InsP_3Rs$, influencing Ca^{2+} signalling [8]. Notably, Ca^{2+} signals also feedback to regulate RAS activity [9].

Like KRAS, Ca^{2+} signals have pleiotropic effects controlling cellular life and death decisions [4]. As such, dysregulated Ca^{2+} signalling pathways contribute to the altered activity of cell processes underlying cancer [4,5,10]. In particular, Ca^{2+} signals sustain the cell cycle at G_1/S and G_2/M transitions [4,11,12] and induce apoptosis via mitochondrial Ca^{2+} overload [4,10]. Ca^{2+} signals also regulate the cell migration and invasion associated with tumour metastasis [13–15].

Increases in cytosolic Ca^{2+} are generated through release from intracellular stores and/or influx across the plasmalemma. While Ca^{2+} signalling pathways centred on the endoplasmic reticulum (ER) have primarily been invoked in the altered cell physiology of cancer cells, a

prominent role for Ca^{2+} influx across the plasmalemma is now also emerging [16]. Indeed, the Ca^{2+} influx pathway engaged following depletion of the ER Ca^{2+} store (Store-Operated Ca^{2+} Entry; SOCE) contributes to the regulation of cell proliferation, migration and apoptosis [16] – cell processes modified in cancer cells [4,5,17]. Further supporting a role for SOCE in these processes, altered SOCE and expression and activity of its underlying mediators STIM and ORAI are observed in cancer, including in colorectal cancer [18,19] and melanoma [15,20]. Indeed, STIM1 and ORAI1, have been found to control G_1/S transition in cervical cancer SiHa cells [11]. Moreover, inhibition of STIM1 and ORAI1 via siRNA impairs migration of breast [21,22] and cervical cancer cells [23], and overexpression of STIM1 favours invasion [18].

Despite these advances in identifying altered intracellular Ca^{2+} regulation as a hallmark of cancer, the interaction between Ca^{2+} homeostasis/signalling and cellular transformation induced by a particular oncogenic mutation remains poorly explored. While analysis of tumour-derived and normal cells of the same tissue origin or neighbouring to the tumour has provided important information [15,19], these controls may not adequately reflect the cell type/genetic status of the cell type of origin. Further inconsistencies are observed on analysis of transformed cells from tumours at different stages and origins as well as whether the original tumour or its metastasis are analysed [24,25]. An approach successfully used to circumvent these issues in cellular diversity has been to determine the consequences of genetic deletion of specific mutated oncogenic alleles from a transformed cell [26,27]. Comparison of isogenic cell line pairs thus generated provides specific information regarding the interaction between the mutated allele and the phenotype studied. Given the frequency of *KRAS* mutations in colorectal cancer, we have used this approach to probe functional interactions between this GTPase and Ca^{2+} handling. We previously demonstrated that through suppression of inositol 1,4,5-trisphosphate receptor ($InsP_3R$) expression, cells harbouring a mutated *KRAS* allele exhibited a reduction in both Ca^{2+} signalling induced by an $InsP_3$-generating agonist and of mitochondrial Ca^{2+} uptake, which together served to protect from death-inducing stimuli [28]. Given the growing body of evidence supporting a role of Ca^{2+} influx in cell proliferation and cell migration in cancer, including in CRC, we here examined whether Ca^{2+} entry mechanisms were also a target of activated KRAS. As previously, we analysed CRC cell line pairs that were isogenic albeit for a single copy of

oncogenic *KRAS* (encoding KRAS^{G13D}), which was deleted by homologous recombination [26]. Use of these cell line pairs thus allows the selective analysis of the influence of the oncogenic KRAS on cell phenotype without the confounding effects observed in studies in which KRAS is expressed at supraphysiological levels, such as induction of cell senescence [27]. Using biochemical, fluorometric and electrophysiological approaches, we demonstrate that KRAS^{G13D} expression in the isogenic CRC cell model was associated with reduced SOCE and I_{CRAC} as well as remodelled expression of STIM proteins. KRAS^{G13D} expression was also associated with a reduced sensitivity to cell death induced by activation of SOCE. The lower Ca^{2+} entry in KRAS^{G13D} expressing cells was augmented to the levels in the KRAS-deficient cells by STIM1 overexpression, indicating that STIM1 expression is a direct downstream target of KRAS^{G13D} in CRCs. Targeting KRAS/Ca^{2+} signalling interactions pathway may thus provide a strategy to intervene in the development of CRC.

2. Methods

2.1. Materials

Salts for physiological recordings were of the highest grade and purchased from Sigma-Aldrich, Fisher Scientific or BDH. Na-methanesulfonate, Adenosine 5′ -triphosphate magnesium salt and Cs-methanesulfonate and salts for internal solutions were from Sigma (St. Louis, MO, USA). Cs-BAPTA and Ca^{2+}-sensitive fluorescent indicators were from Invitrogen (Eugene, OR, USA). Sources for other reagents used are indicated where described.

2.2. Cell culture

HCT 116 and DLD-1 cells (both *KRAS*$^{G13D/WT}$) and their respective isogenic derivatives HKH-2 and DKO-4 (both *KRAS*$^{-/WT}$) were a kind gift of S. Shirasawa (Fukuoka University, Japan) and have been previously described [26]. Cells were cultured in DMEM (Life Technologies, Carlsbad, CA, USA), containing 10 % heat-inactivated foetal bovine serum (FBS) (Invitrogen), 1 % penicillin/streptomycin solution (5 units penicillin, 55 µg streptomycin) (Sigma, Dorset, UK). Cells were maintained at 37 °C with 5 % CO_2 in saturated humidity and passaged upon reaching 80-90 % confluency.

2.3. Imaging of cytosolic Ca^{2+}

Imaging and analysis of cytosolic Ca^{2+} levels was performed as previously described [28]. Briefly, cells were seeded onto poly-L-lysine-coated coverslips at equivalent densities and imaged after 48 h. Imaging was carried out using Ca^{2+} containing and Ca^{2+} free HEPES buffered solutions as previously described [29] and included in the supplementary information. Prior to each experiment, coverslips were mounted into stainless steel imaging chambers and loaded with fura-2 AM diluted in Ca^{2+} containing imaging buffer (Life Technologies; 2 µM for 30 min), followed by de-esterification in Ca^{2+}-free buffer for 30 min during which thapsigargin (Tg, 2 µM; SIGMA) was included for the final 15 min. Coverslips were imaged on the stage of a Nikon Eclipse TE200 inverted epifluorescence microscope equipped with a Nikon PlanFluor 20x/0.75 NA multi immersion objective (Nikon, Kingston Upon Thames, Surrey, UK). Excitation light at 340 and 380 nm was selected using a motorised filter wheel (Sutter Industries, Novato, CA, USA) at a frequency of 1 image pair every 3 s with an exposure of 200 ms and emitted light was selected using a 400 nm dichroic mirror and filtered through a 460 nm long pass filter. Images were captured using a Hamamatsu ORCA ER Charge-Coupled Device (CCD) camera. Three coverslips per cell type were imaged per day on 3 separate days.

2.4. Whole-cell patch clamp electrophysiology

Whole-cell patch clamp recordings were performed at room temperature using an Axopatch 200B and Digidata 1440A (Axon Instruments) previously published [30]. Internal and bath solutions were as previously described [30] and as provided in the supplementary information. Clampfit 10.1 software was used for data analysis. Pipettes were pulled from borosilicate glass capillaries (World Precision Instruments, Inc. Sarasota, FL) with a P-1000 Flaming/Brown micropipette puller (Sutter Instrument Company, Novato, CA) and polished with DMF1000 (World Precision Instruments, Inc. Sarasota, FL) to a resistance of 2-4 MΩ when filled with pipette solutions. Immediately before the experiments, cells were washed with bath solution. Only cells with tight seals (>16 GΩ) were selected to break in. Cells were maintained at a 0 mV holding potential during experiments and subjected to voltage ramps

from +100 to −140 mV lasting 250 ms every 2 s. “Reverse” ramps were designed to inhibit Na^+ channels potentially expressed in these cells. High $MgCl_2$ (8 mM) was included in the patch pipette to inhibit TRPM7 currents. All experiments were performed at room temperature.

2.5. Transient transfection

For expression of STIM1 in HCT 116 cells, plasmids were used encoding YFP-STIM1 (kind gift of Prof S. Muallem, NIDCR, Bethesda, USA) or YFP (purchased from Clontech). Cells were transfected using JetPei (Polyplus Transfection) following the manufacturer’s instructions 24 h post seeding the cells onto glass coverslips. Transfection efficiency was ~50 %.

2.6. Mn^{2+} quench imaging

Cells were seeded as described for ratiometric imaging and imaged using an Olympus IX81 inverted epifluorescence microscope equipped with an Olympus UPlanSApo 20x/0.75 NA air objective. Wavelengths for excitation of fura-2 in its Ca^{2+} free (380/10 nm), Ca^{2+}-bound (340/10 nm), and Ca^{2+} insensitive isosbestic (360/4 nm) forms were selected using a Polychrome V monochromator. Emitted light was filtered through a 400 nm dichroic mirror and an emission filter wheel. Images were captured using a Hamamatsu ORCA ER CCD camera. The imaging system was controlled by the Olympus CellR software. When imaging YFP-transfected cells, a reference image of the YFP-positive cells was captured using 480 nm excitation and filtering through a 520 nm long-pass filter.

2.7. Immunoblotting

Immunoblotting was performed as previously described with minor modifications [28]. Cells were seeded and harvested after 48 h or at the times specified. 15 to 30 µg of protein lysate for each sample, quantitated using a bincinchoninic acid (BCA) protein assay kit (Thermo Scientific), was loaded per lane onto self-poured 7 % SDS- polyacrylamide gels or 4-12 % Bis-Tris gradient gels (NuPage). Proteins were transferred from the gels onto polyvinilidene fluoride (PVDF) membranes and probed with the following antibodies: anti-STIM1 (dilution

1:1000, BD Bioscience #610954), anti-STIM2 (dilution 1:1000, Abcam #ab181258) and anti-calnexin (dilution 1:20000, Sigma #C4731). Detection of immunoreactive bands was carried out after incubation with horseradish peroxidase (HRP)-conjugated secondary antibodies (dil. 1:10,000) using Enhanced Chemiluminescence (ECL) reagent (Thermo Scientific) or using fluorescence-based detection (Odyssey CLx, LI-COR) and secondary antibodies conjugated to fluorophores excited at 680 nm and 800 nm.

2.8. Immunofluorescence

Cells were seeded as described for cytosolic Ca^{2+} imaging. 48 h post-seeding, cells were processed for immunofluorescence analysis as previously described [28]. Briefly, after washing in PBS, cells were fixed with 2% paraformaldehyde 0.05% glutaraldehyde. Cells were then permeabilised in PBS containing 0.2 % TRITON X-100 after which non-specific sites were blocked with Chemiblocker (5% in PBS/0.1% TRITON X-100; EMD Millipore). Cells were then labelled with primary antibodies against STIM-1 (BD Bioscience; 1:100) and calnexin (SIGMA; 1:500) diluted in blocking buffer overnight at 4 °C. After washing for 1 h, coverslips were incubated with Alexa-Fluor conjugated secondary antibody (dilution 1:500; Thermo Fisher). Coverslips were then mounted onto glass slides with Vectashield mounting agent containing DAPI (Vector laboratories). Cells were imaged using an Olympus FV1000 point-scanning confocal imaging system configured on an Olympus IX81 inverted microscope equipped with an Olympus PlanSApo 60x/1.35 oil objective.

2.9. Flow Cytometry

Analysis of sub-G1 DNA content was performed as previously described [28] with minor modifications. Cells in the medium were collected and pooled with cells that remained attached to their substrate that were harvested by trypsinization. After washing in PBS, cells were fixed with 70% ethanol and then treated with RNase and stained with propidium iodide (PI). Stained cells were analysed with a Becton Dickinson Canto II AIG flow cytometer (Oxford, UK). Single cells in suspension were excited at 488 nm by an argon laser and analysed according to the intensity of emitted fluorescence at 572 nm.

2.10. Gene expression analysis by RT-qPCR

Gene expression was determined as previously described with minor modifications [31]. Briefly, each cell type was plated in 4 wells of a 12 well dish and after culture for 48 h processed independently for RT-qPCR. RNA was extracted using TRI-Reagent (Sigma), and 500 ng RNA was primed with random hexamers and reverse transcribed using SuperScript II (Life Technologies) following the manufacturer's instructions. Target gene expression in triplicate samples were analyzed by real time quantitative PCR on a CFX384 (Bio-Rad) using the Platinum SYBR Green qPCR SuperMix-UDG (Life Technologies) and target-specific oligonucleotide primers (sequences given in Supplemental Information). The experiment was repeated on 6 occasions. Gene expression was normalized to the geometric mean of the expression of 3 reference genes (*PABP, ELL2 and GAPDH*) according to the ΔΔCt method [32]. Reference genes were selected from a panel of 10 genes (not associated with Ca^{2+} signalling) that were found through a bioinformatics analysis of 4 published microarray datasets to be stably expressed in HCT116 cells exposed to different growth inhibiting drugs (GEO database: GSE19199, GSE15395, GSE14103, GSE11578). 3 genes out of the panel of 10 that exhibited the greatest stability under the conditions of our experiments were identified using the GeNorm algorithm and used for our analysis [32].

2.10. Statistical analysis

Statistical analyses were performed using GraphPad Prism 6. Data represents a minimum of 3 independent biological replicates, sample numbers for each experiment indicated in the figure legend. For testing statistical significance of three or more conditions, the means were compared by analysis of variance (ANOVA) followed by post-hoc Holm-Sidak's Multiple Comparison test (for testing statistical significance between groups of the same dataset, illustrated with a line between groups). A one-sample Student's *t*-test was used for establishing significance between two experimental conditions within a data set. Data was taken as significant when P was less than 0.05, which was represented as *. P-values less than 0.01, 0.001, 0.0001 were represented by **, *** and ****, respectively.

3. Results

3. 1. K-Ras^{G13D} suppresses SOCE in colorectal cancer cell lines

Using the HCT 116 colorectal cancer cell line (possessing the oncogenic *KRAS* allele encoding KRAS^{G13D}) and its isogenic derivative HKH-2 (oncogenic allele ablated by homologous recombination), we previously identified that the presence of oncogenic KRAS and protection against apoptotic stimuli was associated with reduced $InsP_3$-mediated Ca^{2+} release from intracellular ER stores, ER Ca^{2+} levels and mitochondrial Ca^{2+} uptake [28]. Given the importance of SOCE in cancer cell processes and maintenance of ER Ca^{2+} levels, which are altered in KRAS mutated cells, SOCE was examined in the same HCT 116 and HKH-2 cell pair. To this end, experimental strategies that allowed isolation of SOCE from other Ca^{2+} signalling mechanisms were employed. SOCE was first investigated by measuring Ca^{2+} influx across the PM during a period of Ca^{2+} re-addition following depletion of ER Ca^{2+} with the irreversible inhibitor of the SERCA pump thapsigargin (Tg). Application of Tg to cells bathed in Ca^{2+}-free imaging buffer induced a typical increase in cytosolic Ca^{2+} concentration $[Ca^{2+}]_i$ due to uncovering of the passive leak of Ca^{2+} from the ER, which as previously reported was greater in HKH-2 cells than in HCT116 cells (Fig. 1Ai and as in [28]). After 10 min treatment with Tg to allow depletion of the ER Ca^{2+} store, cells were superfused with Ca^{2+}-containing imaging buffer, thereby initiating SOCE. The resulting increase in $[Ca^{2+}]_i$ reached a peak amplitude and magnitude (integrated signal) that was no different between the two cell types (Fig. S1A). As the peak amplitude of the entry Ca^{2+} signal is influenced by feedback mechanisms, Ca^{2+} buffering and clearance mechanisms, the rate of rise of the Ca^{2+} entry signal, which provides a more direct measure of Ca^{2+} flux [33], was also determined. To this end, the Ca^{2+} entry signals in both HCT 116 and HKH-2 cells were normalized to the maximal $[Ca^{2+}]_i$ level (Fig 1Aii) and the first derivative was obtained (Fig. 1Aiii and iv). The maximal rate of Ca^{2+} influx was significantly greater in HKH-2 cells than in HCT 116 cells (Fig. 1Aiv). Consistent with the reduced Ca^{2+} entry following store depletion with Tg in HCT 116 cells, these cells were protected against cell death resulting from chronic Tg application when compared to HKH-2 cells (Fig S2).

To further probe SOCE in isolation from the Ca^{2+} homeostatic mechanisms described above, we assessed the rate of manganese (Mn^{2+}) influx following store depletion with Tg. Mn^{2+} serves as a surrogate for Ca^{2+} permeating SOCE channels, but is a poor substrate for Ca^{2+} dependent ATPases, and as such is not efficiently extruded across the plasmalemma. The influx of Mn^{2+} was monitored through the quenching of fura-2 fluorescence, determined when excited at its Ca^{2+}-independent isosbestic point (~360 nm). ER stores were depleted of Ca^{2+} with Tg during the de-esterification step of fura-2 loading prior to imaging. Cells were then imaged in Ca^{2+}- and, $MnCl_2$-free imaging buffer to obtain a baseline level of fura-2 fluorescence. To monitor the activity of SOCE, $MnCl_2$ (2 mM) in Ca^{2+}-free imaging buffer was then superfused over the cells. While $MnCl_2$ addition induced a mono-exponential decline in fura-2 fluorescence in both cell types (Fig. 1Bi), the rate of decline, illustrated by the maximal derivative of the fura-2 quench by Mn^{2+}, was significantly greater in HKH-2 cells than in HCT 116 cells (Fig. 1Bii and iii).

Basal Ca^{2+} influx (i.e. Ca^{2+} entry occurring in resting HCT 116 and HKH 2 cells with replete Ca^{2+} stores) (Fig S1B), and Ca^{2+} influx following agonist application (ATP; partial store depletion) (Fig S1C) were also assessed by Mn^{2+} quench of fura-2, and found to be lower in the HCT 116 cells than HKH-2 cells, further confirming an influence of $KRAS^{G13D}$ on SOCE.

3.2. $KRAS^{G13D}$ suppresses I_{CRAC} in CRC cell lines

In non-excitable cells such as the colorectal cancer cells examined in this study, Ca^{2+} entry across the plasmalemma occurs via both SOCE dependent and independent pathways. Experiments were therefore carried out to establish that SOCE was specifically affected by loss of mutated KRAS. To this end, the defining and underlying current of SOCE, $I_{CRAC,}$ was measured in HCT 116 and HKH-2 cells by whole cell patch clamp electrophysiology. I_{CRAC} was induced by Ca^{2+} store depletion with BAPTA (20 mM), included in the pipette solution and cells were bathed in bath solution containing 20 mM Ca^{2+} to maximize inward Ca^{2+} currents [30]. The recordings in Fig 2Ai and ii, from HCT 116 and HKH-2 cells respectively, show a slowly developing inward current that was activated within 3-4 min of whole cell configuration being achieved. The current was substantially augmented by replacement of the Ca^{2+} containing bath solution with divalent free (DVF) solution, which results in Na^{+} being the principal charge carrier. The recordings also show a rapid loss of potentiation of

the Na^+ current during the short time windows of exposure to DVF. This loss of potential is experimentally observed as a rapid increase in inward current caused by exposure to DVF (i.e. Na^+ influx), followed by a progressive decline in the current during the DVF application. During the first exposure to DVF immediately after break-in, where I_{CRAC} was negligible, a small current which does not depotentiate, likely representing leak, was observed. A second DVF pulse was applied after I_{CRAC} had fully developed resulting in a relatively large Na^+ current that showed a rapid depotentiation during the short time windows of exposure to DVF, a defining biophysical signature of I_{CRAC} [30,34] (Fig 2Ai and ii). The sensitivity of the current recorded in both cell lines to Gd^{3+} (5 μM) supports the identity of the current as I_{CRAC} (Fig. 2A). Current-voltage relationships for the currents recorded in HCT 116 and HKH-2 cells are also shown in Fig 2Aiii. These data indicate inward rectification of the current and a positive reversal potential (+60 mV), which are known features of I_{CRAC} [30,35]. Notably, the magnitude of the current recorded at -100 mV was significantly greater in HKH-2 cells than in HCT 116 cells (Fig. 2Aiv).

To verify whether reduced I_{CRAC} was a common feature of $KRAS^{G13D}$ expressing cells, we measured I_{CRAC} in a second $KRAS^{G13D}$-expressing cell line, DLD-1, and its isogenic derivative DKO-4 (in which the oncogenic *KRAS* allele was also deleted by homologous recombination, [26]) (Fig. 2B). Similar protocols were used for the DLD-1/DKO-4 cell line pair as were used for HCT/HKH-2 in Fig 2A. Although currents were generally greater in both DLD-1 and DKO-4 cells (Fig 2Bi-iii) compared to HCT 116 and HKH-2 cells, characteristic features of I_{CRAC} (i.e. inward rectification, positive reversal potential and depotentiation in DVF solutions) were also observed in DLD-1 and DKO-4 cells. As shown in Fig. 2Biv, I_{CRAC} was lower in the $KRAS^{G13D}$-expressing DLD-1 cells than in the DKO-4 cells (Fig. 2Biv).

Together, the data obtained from fura-2 measurements (Fig. 1) and electrophysiological recordings of I_{CRAC} (Fig. 2) show that loss of the oncogenic *KRAS* allele in CRC cell lines results in increased SOCE.

3.3. STIM1 and STIM2 expression is regulated by $KRAS^{G13D}$ in CRC cell lines

STIM proteins are essential for coupling ER Ca^{2+} store depletion with Ca^{2+} entry channels on the plasma membrane. To assess whether the enhanced SOCE observed following deletion of oncogenic *KRAS* allele was due to altered STIM expression, STIM1 and STIM2 protein and mRNA levels were assessed by immunoblotting and RT-qPCR, respectively, in HCT 116 and HKH-2 cells. STIM1 protein and mRNA levels were significantly greater in HKH-2 compared to HCT 116 cells (Fig. 3Ai-iii). STIM2 protein levels were also differentially expressed between HCT 116 and HKH-2 cells, although STIM2 levels were significantly lower in the absence of $KRAS^{G13D}$ (Fig. 3Aiv and v). mRNA levels of STIM2 were however unchanged (Fig. 3Avi).

Given the greater I_{CRAC} in DKO-4 cells compared to their isogenic DLD-1 counterparts harbouring an oncogenic *KRAS* allele, the expression of STIM1 and 2 was also investigated in these cells. The expression profile of STIM1 and 2 in the DLD-1/DKO-4 cell line pair was different than between the HCT 116/HKH-2 cell lines (Fig. 3B). Specifically, STIM1 protein expression was significantly greater in DLD-1 than DKO-4 cells (Fig. 3Bi and ii). In contrast to that observed for HCT 116 and HKH-2 cells, STIM2 protein was more abundant in DKO-4 cells compared to DLD-1 (Fig. 3Bi and iv). mRNA levels of STIM1 and STIM2 were similar between DLD-1 and DKO-4 cell lines (Fig. 3Biii and v).

3.4. YFP-STIM1 expression is sufficient to elevate SOCE in the HCT 116 cells

The correlation between increased STIM1 expression, enhanced SOCE/I_{CRAC} and loss of $KRAS^{G13D}$ between HCT 116 and HKH-2 cells suggested a causal role of STIM1 in determining SOCE/I_{CRAC} activity. Whether increasing STIM1 levels was sufficient to bring about an increase in SOCE/I_{CRAC} in HCT 116 was therefore tested. To this end, yellow fluorescent protein (YFP)-tagged STIM1 (YFP-STIM1) was overexpressed in HCT 116 cells and SOCE was measured. HCT 116 cells were transfected with YFP-STIM1 or with YFP alone, which was used as a transfection control (Fig. S3). YFP-STIM1 exhibited the expected ER distribution, co-localising with ER-localised chaperone calnexin (FIG. S3 top row, right panel). SOCE was analysed in YFP-STIM1- and YFP-expressing cells by Mn^{2+} quench of fura-2, as described above (Fig. 4i). The maximal derivative of the rate of Mn^{2+} quench of fura-2 in HCT 116 cells was substantially increased by YFP-STIM1 expression (Fig. 4ii and iii), reaching levels approaching that observed in HKH-2 cells (Fig. 1B.). These data are consistent with the

hypothesis that a difference in STIM1 expression underlies the altered SOCE between HCT 116 and HKH-2 cells.

3.5. Expression of STIM proteins is regulated by ERK signalling in the HCT 116 CRC cell line

$KRAS^{G13D}$-expressing HCT 116 cells exhibit increased ERK pathway activation compared to their HKH-2 isogenic derivatives [28,36]. Given the role of ERK signalling in regulation of gene expression, we next investigated whether this signalling pathway contributed to the regulation of STIM expression in HCT 116 cells. ERK signalling was inhibited in HCT 116 cells by application of the MEK inhibitor (48 h with 5 μM PD184352; an exposure duration and dose determined to be sufficient to elicit an increase in STIM1 expression, Fig. S4). Since MEK lies directly upstream of ERK1/2, inhibition of its activation prevents ERK1/2 activation as well as downstream signalling [37]. PD184352 application resulted in a significant increase in STIM1 protein and mRNA, reaching levels comparable with those expressed by HKH-2 cells (Fig 5Ai-iii). Protein levels of STIM2 in HCT 116 cells were also altered by PD184352 application, so that its expression was reduced to levels comparable to that for HKH-2 cells (Fig. 5B). PD184352 treatment did not influence mRNA abundance of STIM2 in HCT 116 cells.

Together, these data indicate that STIM expression and SOCE lie downstream of $KRAS^{G13D}$ in CRC cell lines.

4. Discussion

Here we established a functional interaction between oncogenic KRAS and SOCE in two isogenic pairs of CRC cell lines. We determined that the presence of oncogenic KRAS was associated with a suppression of SOCE and its underlying current I_{CRAC}. Consistent with these observations, the expression of the STIM proteins required for transduction of the state of filling of the ER to the plasma membrane to activate Ca^{2+} entry was remodelled in cancer cells expressing mutated KRAS. Ectopic expression of STIM1 in $KRAS^{G13D}$ cells was sufficient to enhance SOCE, demonstrating the role of reduced STIM1 in the Ca^{2+} handling phenotype of these cells.

SOCE is fundamental to intracellular Ca^{2+} signalling and homeostasis and as such is emerging as an important contributor to the hallmarks of transformed cells [5,16] Indeed, SOCE is augmented and expression of its molecular mediators, STIM1 and ORAI1 are increased in a range of different cancer types, including colorectal cancer [18,19]. Moreover, the expression level of components of the SOCE pathway directly correlates with tumour cell proliferation, aggressiveness and invasiveness in the above-mentioned reports, highlighting a role for changes in expression, and not just activity, of SOCE and its regulators. In contrast to these studies, we found that the presence of the oncogenic *KRAS* allele was associated with reduced SOCE and its underlying current I_{CRAC}. Given the reported requirement for Ca^{2+} influx for cell migration and proliferation [11,13,14], these observations might seem counterintuitive, although a recent study found SOCE to also be diminished in invasive melanoma cells compared a non-invasive form of the disease [15]. Divergent effects of Ca^{2+} entry on cell proliferation and metastasis have however been reported [5,16,38]. Possible explanations for these discrepancies included cell type origin/tumour type, inappropriate controls, stage of transformation or whether the original tumour or metastasis is analysed. Indeed, the requirement for Ca^{2+} signals during oncogenic transformation likely varies according to the stage of differentiation and functional requirements of the cell [4,5,38]. In colorectal cancer (CRC) for example, STIM1 was differentially important between colonic and rectal cancers [39].

The data showing repression of Ca^{2+} influx in the presence of activated KRAS described here are in line with the widely reported anti-apoptotic role of reduced ER-based Ca^{2+} signalling mechanisms observed in transformed cells [4,10]. According to this paradigm, reduced Ca^{2+} release from the ER and lesser Ca^{2+} transfer to the mitochondria acts as a mechanism to protect transformed cells from apoptotic cell death. Several mechanisms have been proposed to underlie the reduced ER Ca^{2+} release, including a reduction in ER luminal Ca^{2+} and altered expression or activity of $InsP_3Rs$ [4,10,28]. Given that SOCE participates in maintaining ER store Ca^{2+} content, the reduction in SOCE described here could also contribute to reducing the pool of releasable Ca^{2+}. Notably, in a previous study in which we analysed Ca^{2+} handling in the same isogenic cell line pairs as described here, activated KRAS expression corresponded with reduced ER luminal Ca^{2+} [28]. Comparison of CRC cells with

normal colon mucosa cells also revealed that despite increased SOCE in the cancer counterpart, store content was diminished [19], consistent with our previous results. Here we find that SOCE contributes to the differences in sensitivity to cell death between the HCT 116 and HKH-2 cells. In particular, cell death induced by Tg, which has previously been shown to induce apoptosis in a SOCE-dependent manner [40] was greater in the HKH-2 cells than in the oncogenic KRAS-expressing HCT 116 cells. A direct link between Ca^{2+} entry and cell survival that is dependent upon mitochondrial Ca^{2+} uptake has also recently been delineated. STIM proteins directly regulate and are themselves regulated by the mitochondrial Ca^{2+} uniporter (MCU; the channel responsible for mitochondrial Ca^{2+} uptake). Specifically, expression of MCU is decreased in cells with reduced STIM1 [41] and in turn SOCE is lower following MCU silencing [42].

STIM1 and 2 play different roles in regulation of Ca^{2+} influx. As such, the relative abundance of STIM1 and/or STIM2, as well as their association with ORAI1 [19,43], define their effect on SOCE and cell function. Here we found that while STIM1 expression was lower in oncogenic KRAS-expressing HCT 116 cells compared to their mutated *KRAS* deficient isogenic derivatives, the expression of STIM2 was greater. This raises the possibility that it is the reciprocal regulation of these two STIM isoforms, and not only a change in STIM1, that contributes to the altered SOCE regulation observed. Indeed, differences in the STIM-ORAI-activating regions (SOAR) of STIM1 and 2 are responsible for the differential coupling of the two STIM isoforms with ORAI1, in which STIM1 acts as a full ORAI1 agonist and STIM2 exerts an inhibitory effect [44]. Thus, the lower SOCE observed in HCT 116 compared to HKH-2 cells may be due not only to lower STIM1–mediated ORAI activation but also increased inhibition by STIM2. Overexpression of STIM1 was however sufficient to enhance SOCE in HCT116 cells, indicating the importance of its repressed expression in the phenotype of these cells. In accordance with this notion, STIM2 was recently found to be overexpressed in melanoma [45] and in CRC [46], with its presence associated with a less invasive phenotype. It is possible that, in HCT 116 cells and in cancers with a high STIM2/STIM1 ratio, SOCE is decreased to a basal level, which impairs apoptosis yet provides the Ca^{2+} necessary to sustain the cell cycle [11].

The repressive effect of oncogenic KRAS on SOCE in both DLD-1 and HCT 116 cells suggests reduced SOCE is a feature of CRC cells expressing mutated KRAS. However, a different

expression profile of STIM1 and 2 in the HCT 116/HKH-2 and DLD-1/DKO-4 cell line pairs was observed that would possibly indicate different mechanisms for coupling KRAS activity and expression of STIM1/2 between HCT 116 and DLD-1 cells. These differences may in part be explained by the different signalling pathways engaged downstream of activated KRAS in HCT 116 and DLD-1 cells. While the ERK pathway is principally engaged in HCT 116 cells and was shown here to regulate STIM1/2 expression, the PI3K-AKT pathway dominates in DLD-1 cells [37]. Despite these differences, HCT 116 and DLD-1 cells exhibit properties of the transformed phenotype, including for example increased cell proliferation and avoidance of cell death [26,28]. Consistent with this hypothesis, Schmidt et al. reported that in ovarian cancer cells, STIM1 expression and SOCE were under the control of AKT [47], which is increased in activity in DLD-1 cells. How MAPK signalling pathways couple to STIM expression in the cell lines studied remains to be determined. STIM1 expression has been shown to be under the control of the early growth response (EGR) family of zinc finger transcription factors [48]. Since these transcription factors lie downstream of ERK, which is elevated in activity in HCT116 cells, it is unlikely however that they are involved in regulation of STIM expression in these cells. Kinase signalling pathways also regulate STIM1 activity through a direct phosphorylation in a cell cycle dependent manner [49]. These mechanisnms were not studied here however but may represent a further mechansism to couple Ca^{2+} entry pathways and cell proliferation in cancer. Interestingly, STIM1 expression and SOCE have also been correlated with ERK activation, which in light of our findigs suggests a mechanism for feedback regulation. In particular, in cell lines from invasive melanoma, which exhibited enhanced STIM1 and SOCE, thapsigargin promoted ERK activation in a manner that was dependent upon STIM1 expression [20]. Similarly, in epidermal keratinocytes, SOCE inhibition prevented ERK phosphorylation and IL-8 production induced by IL-9 [50].

In conclusion, our findings identify SOCE and its molecular components as targets of oncogenic KRAS in colorectal cancer cells. Together with our identification of reduced $InsP_3R$ abundance and ER Ca^{2+} release, also in the same oncogenic KRAS expressing cells, and the growing body of evidence from other studies describing altered Ca^{2+} handling in cancer, our findings here underlie the important contribution of remodelling of the Ca^{2+} signalling toolkit in disease to support and facilitate the required alterations in physiology – in this

case cancerogenesis [4,5,51]. While our data point to an important role of altered $InsP_3R$ signalling, mitochondrial Ca^{2+} uptake and SOCE in colorectal cancer cell lines harbouring oncogenic KRAS, other signalling pathways and cell processes, modified through the process of oncogenic transformation, also contribute to the phenotype of these cells. The rescue of SOCE by STIM1 overexpression however indicates the direct contribution of STIM1 to the SOCE phenotype observed. Whether remodelled SOCE, altered expression of STIM proteins, or other components of the SOCE machinery contribute to transformation of other cancer types in which activated KRAS mutations are expressed remains to be established however. It will also be important to determine the contribution of SOCE remodelling and SOCE regulated processes during the different stages of oncogenesis. Addressing these questions together with the knowledge of the role of SOCE in cancer provided here will provide new STIM/SOCE-specific avenues for the design of cancer therapeutics.

Duality of Interest

The authors declare that they do not have any potential conflicts relevant to this study.

Acknowledgements

C.P. was funded by the Aldobrandini Studentship of St John's College, Cambridge, UK. The H.L.R. laboratories are supported by the Babraham Institute, the Biotechnology and Biological Sciences Research Council (BBSRC) [Epigenetics and Signalling ISPGs (Institute Strategic Programme Grant)]. HLR also received funding from an Odysseus Award from the Research Foundation Flanders (FWO) and The Royal Society (University Research Fellowship to HLR). MT received funding from National Institutes of Health Grants R01 HL-123364, R01 HL-097111, and R21 AG-050072, and grant NPRP8-110-3-021 from the Qatar National Research Fund (QNRF). We are grateful to Prof Shmuel Muallem (NIDCR, Bethesda, USA) for the YFP-tagged STIM1 construct; Dr Simon Walker (Imaging Facility, Babraham Institute, Cambridge, UK), for assistance with imaging, Senji Shirasawa, (Fukuoka University, Japan) for the cell lines and the Roderick laboratory for assistance throughout this work. We thank Simon Andrews (Babraham Bioinformatics Facility) for analysis of microarray datasets and Simon Cook for comments on the manuscript and provision of PD184352.

References

[1] J. Downward, Targeting RAS signalling pathways in cancer therapy., Nat. Rev. Cancer. 3 (2003) 11–22. doi:10.1038/nrc969.

[2] F. Arvelo, F. Sojo, C. Cotte, Biology of colorectal cancer, (2015) 1–20. doi:10.3332/ecancer.2015.520.

[3] H.-C. Chuang, P.-H. Huang, S.K. Kulp, C.-S. Chen, Pharmacological Strategies to Target Oncogenic KRAS Signaling in Pancreatic Cancer., Pharmacol. Res. (2017). doi:10.1016/j.phrs.2017.01.006.

[4] H.L. Roderick, S.J. Cook, Ca2+ signalling checkpoints in cancer: remodelling Ca2+ for cancer cell proliferation and survival, Nat. Rev. Cancer. 8 (2008) 361–375. doi:10.1038/nrc2374.

[5] G.R. Monteith, N. Prevarskaya, S.J. Roberts-Thomson, The calcium–cancer signalling nexus, Nat. Rev. Cancer. (2017). doi:10.1038/nrc.2017.18.

[6] L. Hegedũs, T. Garay, E. Molnár, K. Varga, Á. Bilecz, S. Török, R. Padányi, K. Pászty, M. Wolf, M. Grusch, E. Kállay, B. Döme, W. Berger, B. Hegedũs, A. Enyedi, The plasma membrane Ca(2+) pump PMCA4b inhibits the migratory and metastatic activity of BRAF mutant melanoma cells., Int. J. Cancer. 140 (2017) 2758–2770. doi:10.1002/ijc.30503.

[7] P. Corazao-Rozas, P. Guerreschi, F. André, P.-E. Gabert, S. Lancel, S. Dekiouk, D. Fontaine, M. Tardivel, A. Savina, B. Quesnel, L. Mortier, P. Marchetti, J. Kluza, Mitochondrial oxidative phosphorylation controls cancer cell's life and death decisions upon exposure to MAPK inhibitors., Oncotarget. 7 (2016) 39473–39485. doi:10.18632/oncotarget.7790.

[8] P.J. Sung, F.D. Tsai, H. Vais, H. Court, J. Yang, N. Fehrenbacher, J.K. Foskett, M.R. Philips, Phosphorylated K-Ras limits cell survival by blocking Bcl-xL sensitization of inositol trisphosphate receptors., Proc. Natl. Acad. Sci. U. S. A. 110 (2013) 20593–8. doi:10.1073/pnas.1306431110.

[9] S.A. Walker, P.J. Lockyer, P.J. Cullen, The Ras binary switch: an ideal processor for decoding complex Ca2+ signals?, Biochem. Soc. Trans. 31 (2003) 966–9. doi:10.1042/.

[10] H. Ivanova, M. Kerkhofs, R.M. La Rovere, G. Bultynck, Endoplasmic Reticulum–Mitochondrial Ca2+ Fluxes Underlying Cancer Cell Survival, Front. Oncol. 7 (2017). doi:10.3389/fonc.2017.00070.

[11] Y.-W. Chen, Y.-F. Chen, Y.-T. Chen, W.-T. Chiu, M.-R. Shen, The STIM1-Orai1 pathway of store-operated Ca(2+) entry controls the checkpoint in cell cycle G1/S transition., Sci. Rep. 6 (2016) 22142. doi:10.1038/srep22142.

[12] C.R. Kahl, A.R. Means, Regulation of Cell Cycle Progression by Calcium/Calmodulin-Dependent Pathways, Endocr. Rev. 24 (2003) 719–736. doi:10.1210/er.2003-0008.

[13] F. Tsai, A. Seki, H.W. Yang, A. Hayer, S. Carrasco, T. Meyer, A polarized Ca2+ ,

diacylglycerol, and STIM1 signaling system regulates directed cell migration, 16 (2014) 133–144. doi:10.1038/ncb2906.A.

[14] J. Prudent, N. Popgeorgiev, R. Gadet, M. Deygas, R. Rimokh, G. Gillet, Mitochondrial Ca2+ uptake controls actin cytoskeleton dynamics during cell migration, Sci. Rep. 6 (2016) 36570. doi:10.1038/srep36570.

[15] R. Hooper, X. Zhang, M. Webster, C. Go, J. Kedra, K. Marchbank, D.L. Gill, A.T. Weeraratna, M. Trebak, J. Soboloff, Novel Protein Kinase C-Mediated Control of Orai1 Function in Invasive Melanoma, Mol. Cell. Biol. 35 (2015) 2790–2798. doi:10.1128/MCB.01500-14.

[16] A. Fiorio Pla, K. Kondratska, N. Prevarskaya, STIM and ORAI proteins: crucial roles in hallmarks of cancer, Am. J. Physiol. - Cell Physiol. 310 (2016) C509–C519. doi:10.1152/ajpcell.00364.2015.

[17] D. Hanahan, R.A. Weinberg, Hallmarks of cancer: the next generation., Cell. 144 (2011) 646–74. doi:10.1016/j.cell.2011.02.013.

[18] J.-Y. Wang, J. Sun, M.-Y. Huang, Y.-S. Wang, M.-F. Hou, Y. Sun, H. He, N. Krishna, S.-J. Chiu, S. Lin, S. Yang, W.-C. Chang, STIM1 overexpression promotes colorectal cancer progression, cell motility and COX-2 expression., Oncogene. 34 (2015) 4358–67. doi:10.1038/onc.2014.366.

[19] D. Sobradillo, M. Hernández-Morales, D. Ubierna, M.P. Moyer, L. Núñez, C. Villalobos, A reciprocal shift in transient receptor potential channel 1 (TRPC1) and stromal interaction molecule 2 (STIM2) contributes to Ca2+remodeling and cancer hallmarks in colorectal carcinoma cells, J. Biol. Chem. 289 (2014) 28765–28782. doi:10.1074/jbc.M114.581678.

[20] M. Umemura, E. Baljinnyam, S. Feske, M.S. De Lorenzo, L.H. Xie, X. Feng, K. Oda, A. Makino, T. Fujita, U. Yokoyama, M. Iwatsubo, S. Chen, J.S. Goydos, Y. Ishikawa, K. Iwatsubo, Store-operated Ca2+ entry (SOCE) regulates melanoma proliferation and cell migration, PLoS One. 9 (2014). doi:10.1371/journal.pone.0089292.

[21] N. Yang, Y. Tang, F. Wang, H. Zhang, D. Xu, Y. Shen, S. Sun, G. Yang, Blockade of store-operated Ca2+ entry inhibits hepatocarcinoma cell migration and invasion by regulating focal adhesion turnover, Cancer Lett. 330 (2013) 163–169. doi:10.1016/j.canlet.2012.11.040.

[22] R.K. Motiani, I.F. Abdullaev, M. Trebak, A novel native store-operated calcium channel encoded by Orai3: Selective requirement of Orai3 versus Orai1 in estrogen receptor-positive versus estrogen receptor-negative breast cancer cells, J. Biol. Chem. 285 (2010) 19173–19183. doi:10.1074/jbc.M110.102582.

[23] Y.-F. Chen, W.-T. Chiu, Y.-T. Chen, P.-Y. Lin, H.-J. Huang, C.-Y. Chou, H.-C. Chang, M.-J. Tang, M.-R. Shen, Calcium store sensor stromal-interaction molecule 1-dependent signaling plays an important role in cervical cancer growth, migration, and angiogenesis., Proc. Natl. Acad. Sci. U. S. A. 108 (2011) 15225–30. doi:10.1073/pnas.1103315108.

[24] X.-T. Wang, Y. Nagaba, H.S. Cross, F. Wrba, L. Zhang, S.E. Guggino, The mRNA of L-Type Calcium Channel Elevated in Colon Cancer, Am. J. Physiol. - Cell Physiol. 157 (2000) 1549–1561. doi:10.1016/S0002-9440(10)64792-X.

[25] I. Latour, D.F. Louw, A.M. Beedle, J. Hamid, G.R. Sutherland, G.W. Zamponi, Expression of T-type calcium channel splice variants in human glioma., Glia. 48 (2004) 112–9. doi:10.1002/glia.20063.

[26] S. Shirasawa, M. Furuse, N. Yokoyama, T. Sasazuki, Altered growth of human colon cancer cell lines disrupted at activated Ki-ras., Science. 260 (1993) 85–8.

[27] D.A. Tuveson, A.T. Shaw, N.A. Willis, D.P. Silver, E.L. Jackson, S. Chang, K.L. Mercer, R. Grochow, H. Hock, D. Crowley, S.R. Hingorani, T. Zaks, C. King, M.A. Jacobetz, L. Wang, R.T. Bronson, S.H. Orkin, R.A. DePinho, T. Jacks, Endogenous oncogenic K-rasG12D stimulates proliferation and widespread neoplastic and developmental defects, Cancer Cell. 5 (2004) 375–387. doi:10.1016/S1535-6108(04)00085-6.

[28] C. Pierro, S.J. Cook, T.C. Foets, M.D. Bootman, H.L. Roderick, Oncogenic K-Ras suppresses IP_3-dependent Ca^{2+} release through remodelling of the isoform composition of IP_3Rs and ER luminal Ca^{2+} levels in colorectal cancer cell lines, J Cell Sci. 127 (2014) 1607–1619. doi:10.1242/jcs.141408.

[29] C.M. Peppiatt, A.M. Holmes, J.T. Seo, M.D. Bootman, T.J. Collins, F. McDonald, H.L. Roderick, Calmidazolium and arachidonate activate a calcium entry pathway that is distinct from store-operated calcium influx in HeLa cells., Biochem. J. 381 (2004) 929–39. doi:10.1042/BJ20040097.

[30] X. Zhang, W. Zhang, J.C. González-Cobos, I. Jardin, C. Romanin, K. Matrougui, M. Trebak, J.C. Gonzalez-Cobos, I. Jardin, C. Romanin, K. Matrougui, M. Trebak, Complex role of STIM1 in the activation of store-independent Orai1/3 channels, J. Gen. Physiol. 143 (2014) 345–359. doi:10.1085/jgp.201311084.

[31] B. Thienpont, J.M. Aronsen, E.L. Robinson, H. Okkenhaug, E. Loche, A. Ferrini, P. Brien, K. Alkass, A. Tomasso, A. Agrawal, O. Bergmann, I. Sjaastad, W. Reik, H.L. Roderick, The H3K9 dimethyltransferases EHMT1/2 protect against pathological cardiac hypertrophy, J. Clin. Invest. 127 (2017) 335–348. doi:10.1172/JCI88353.

[32] J. Vandesompele, K. De Preter, F. Pattyn, B. Poppe, N. Van Roy, A. De Paepe, F. Speleman, Accurate normalization of real-time quantitative RT-PCR data by geometric averaging of multiple internal control genes., Genome Biol. 3 (2002) RESEARCH0034. doi:10.1186/gb-2002-3-7-research0034.

[33] G. Bird, W. DeHaven, J. Smyth, Methods for studying store-operated calcium entry, Methods. 46 (2008) 204–212. doi:10.1016/j.ymeth.2008.09.009.Methods.

[34] M. Prakriya, R.S. Lewis, Separation and characterization of currents through store-operated CRAC channels and Mg2+-inhibited cation (MIC) channels., J. Gen. Physiol. 119 (2002) 487–507. doi:10.1085/jgp.20028551.

[35] M. Hoth, R. Penner, Depletion of intracellular calcium stores activates a calcium current in mast cells., Nature. 355 (1992) 353–6. doi:10.1038/355353a0.

[36] S. Vartanian, C. Bentley, M.J. Brauer, L. Li, S. Shirasawa, T. Sasazuki, J.S. Kim, P. Haverty, E. Stawiski, Z. Modrusan, T. Waldman, D. Stokoe, Identification of mutant K-Ras-dependent phenotypes using a panel of isogenic cell lines, J. Biol. Chem. 288 (2013) 2403–2413. doi:10.1074/jbc.M112.394130.

[37] K. Balmanno, S.J. Cook, Tumour cell survival signalling by the ERK1/2 pathway., Cell Death Differ. 16 (2009) 368–77. doi:10.1038/cdd.2008.148.

[38] F. Vanden Abeele, Y. Shuba, M. Roudbaraki, L. Lemonnier, K. Vanoverberghe, P. Mariot, R. Skryma, N. Prevarskaya, Store-operated Ca2+ channels in prostate cancer epithelial cells: Function, regulation, and role in carcinogenesis, Cell Calcium. 33 (2003) 357–373. doi:10.1016/S0143-4160(03)00049-6.

[39] H.S.-C. Wong, W.-C. Chang, Correlation of clinical features and genetic profiles of stromal interaction molecule 1 (STIM1) in colorectal cancers, Oncotarget. 6 (2015) 42169–42182. doi:10.18632/oncotarget.5888.

[40] M. Flourakis, V. Lehen'kyi, B. Beck, M. Raphaël, M. Vandenberghe, F. V Abeele, M. Roudbaraki, G. Lepage, B. Mauroy, C. Romanin, Y. Shuba, R. Skryma, N. Prevarskaya, Orai1 contributes to the establishment of an apoptosis-resistant phenotype in prostate cancer cells, Cell Death Dis. 1 (2010) e75. doi:10.1038/cddis.2010.52.

[41] S. Shanmughapriya, S. Rajan, N.E. Hoffman, X. Zhang, S. Guo, J.E. Kolesar, K.J. Hines, J. Ragheb, N.R. Jog, R. Caricchio, Y. Baba, Y. Zhou, B.A. Kaufman, J.Y. Cheung, T. Kurosaki, D.L. Gill, M. Madesh, Ca2+ signals regulate mitochondrial metabolism by stimulating CREB-mediated expression of the mitochondrial Ca2+ uniporter gene MCU., Sci. Signal. 8 (2015) ra23. doi:10.1126/scisignal.2005673.

[42] S. Tang, X. Wang, Q. Shen, X. Yang, C. Yu, C. Cai, G. Cai, X. Meng, F. Zou, Mitochondrial Ca2+ uniporter is critical for store-operated Ca2+ entry-dependent breast cancer cell migration, Biochem. Biophys. Res. Commun. 458 (2015) 186–193. doi:10.1016/j.bbrc.2015.01.092.

[43] C. Dubois, F. Vanden Abeele, V. Lehen'kyi, D. Gkika, B. Guarmit, G. Lepage, C. Slomianny, A. Borowiec, G. Bidaux, M. Benahmed, Y. Shuba, N. Prevarskaya, Remodeling of Channel-Forming ORAI Proteins Determines an Oncogenic Switch in Prostate Cancer, Cancer Cell. 26 (2014) 19–32. doi:10.1016/j.ccr.2014.04.025.

[44] X. Wang, Y. Wang, Y. Zhou, E. Hendron, S. Mancarella, M.D. Andrake, B.S. Rothberg, J. Soboloff, D.L. Gill, Distinct Orai-coupling domains in STIM1 and STIM2 define the Orai-activating site., Nat. Commun. 5 (2014) 3183. doi:10.1038/ncomms4183.

[45] H. Stanisz, S. Saul, C.S.L. Müller, R. Kappl, B.A. Niemeyer, T. Vogt, M. Hoth, A. Roesch, I. Bogeski, Inverse regulation of melanoma growth and migration by Orai1/STIM2-dependent calcium entry, Pigment Cell Melanoma Res. 27 (2014) 442–453. doi:10.1111/pcmr.12222.

[46] A. Aytes, D.G. Molleví, M. Martinez-Iniesta, M. Nadal, A. Vidal, A. Morales, R. Salazar, G. Capellà, A. Villanueva, Stromal interaction molecule 2 (STIM2) is frequently overexpressed in colorectal tumors and confers a tumor cell growth suppressor

phenotype., Mol. Carcinog. 51 (2012) 746–53. doi:10.1002/mc.20843.

[47] S. Schmidt, G. Liu, G. Liu, W. Yang, S. Honisch, S. Pantelakos, C. Stournaras, A. Hönig, F. Lang, Enhanced Orai1 and STIM1 expression as well as store operated Ca2+ entry in therapy resistant ovary carcinoma cells., Oncotarget. 5 (2014) 4799–810. doi:2035 [pii].

[48] M.F. Ritchie, Y. Zhou, J. Soboloff, Transcriptional mechanisms regulating Ca2+ homeostasis, Cell Calcium. 49 (2011) 314–321. doi:10.1016/j.ceca.2010.10.001.

[49] E. Pozo-Guisado, D.G. Campbell, M. Deak, A. Alvarez-Barrientos, N.A. Morrice, I.S. Alvarez, D.R. Alessi, F.J. Martin-Romero, Phosphorylation of STIM1 at ERK1/2 target sites modulates store-operated calcium entry, J. Cell Sci. 123 (2010) 3084–3093. doi:10.1242/jcs.067215.

[50] C.-H. Hong, K.-L. Chang, H.-J. Wang, H.-S. Yu, C.-H. Lee, IL-9 induces IL-8 production via STIM1 activation and ERK phosphorylation in epidermal keratinocytes: A plausible mechanism of IL-9R in atopic dermatitis, J. Dermatol. Sci. 78 (2015) 206–214. doi:10.1016/j.jdermsci.2015.03.004.

[51] M.J. Berridge, M.D. Bootman, H.L. Roderick, Calcium: Calcium signalling: dynamics, homeostasis and remodelling, Nat. Rev. Mol. Cell Biol. 4 (2003) 517–529. doi:10.1038/nrm1155.

Supplemental information

Composition of buffer solutions

Widefield imaging

Ca^{2+}-containing imaging buffer, pH 7.3

121 mM NaCl (AnalaR Normapur)

5.4 mM KCl (AnalaR Normapur)

0.8 mM $MgCl_2$ (AnalaR Normapur)

1.8 mM $CaCl_2$ (Sigma)

6 mM $NaHCO_3$ (Fischer Scientific)

5.5 mM glucose (Fischer Scientific)

25 mM HEPES (N-(2-Hydroxyethyl)piperazine-N'-(2-ethanesulfonic acid) (Sigma)

5 M NaOH to adjust pH

Ca^{2+}-free imaging buffer, pH 7.3

As Ca^{2+}-containing

-1.8 mM $CaCl_2$

+ 1.8 mM EGTA (Sigma)

5 M NaOH to adjust pH

Whole-cell patch clamp electrophysiology

Store depletion-activated currents

Bath Solution, pH 7.4: 115 mM Na-methanesulfonate, 10 mM CsCl, 1.2 mM $MgSO_4$, 10 mM HEPES, 20 mM $CaCl_2$, and 10 mM glucose (pH adjusted with NaOH).

Pipette Solution, pH 7.2: 115 mM Cs-methanesulfonate, 20 mM Cs-1,2-bis-(2-aminophenoxy)ethane-N,N,N′,N′-tetraacetic acid (Cs-BAPTA), 8 mM $MgCl_2$, and 10 mM HEPES (pH adjusted with CsOH)

ATP-activated currents

Bath Solution, pH 7.4: 115 mM Na-methanesulfonate, 10 mM CsCl, 1.2 mM $MgSO_4$, 10 mM HEPES, 20 mM $CaCl_2$, and 10 mM glucose (pH adjusted with NaOH). 10µM &100µM Mg-ATP was added.

Pipette Solution, pH 7.2: 115 mM Cs-methanesulfonate, 10 mM Cs-1,2-bis-(2-aminophenoxy)ethane-N,N,N′,N′-tetraacetic acid (Cs-BAPTA), 5 mM$CaCl_2$, 8 mM $MgCl_2$, and 10 mM HEPES (pH adjusted with CsOH).

Thapsigargin-activated currents

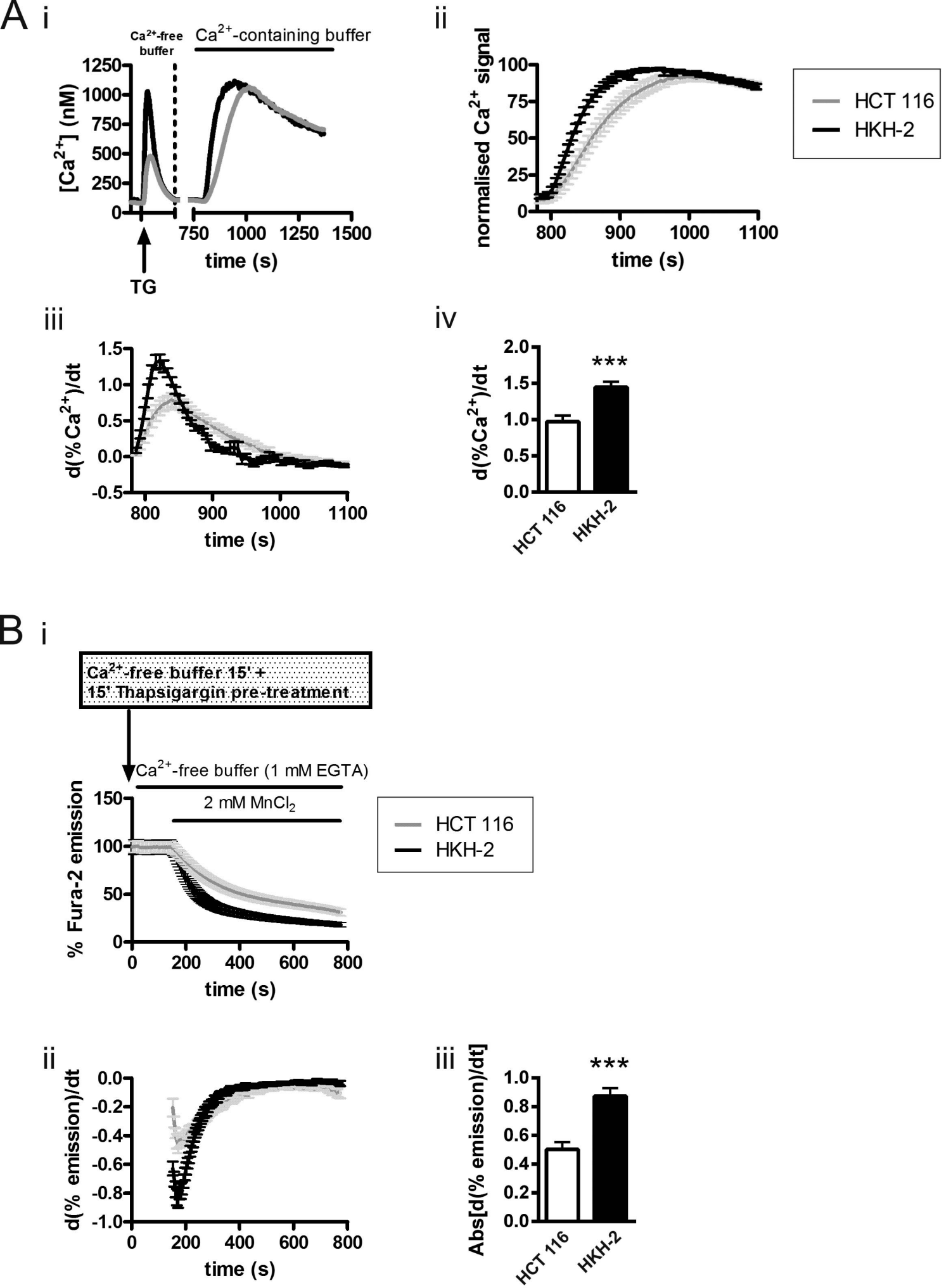
Bath Solution, pH 7.4: 115 mM Na-methanesulfonate, 10 mM CsCl, 1.2 mM $MgSO_4$, 10 mM HEPES, 20 mM $CaCl_2$, and 10 mM glucose (pH adjusted with NaOH). 2µM Thapsigargin was added.

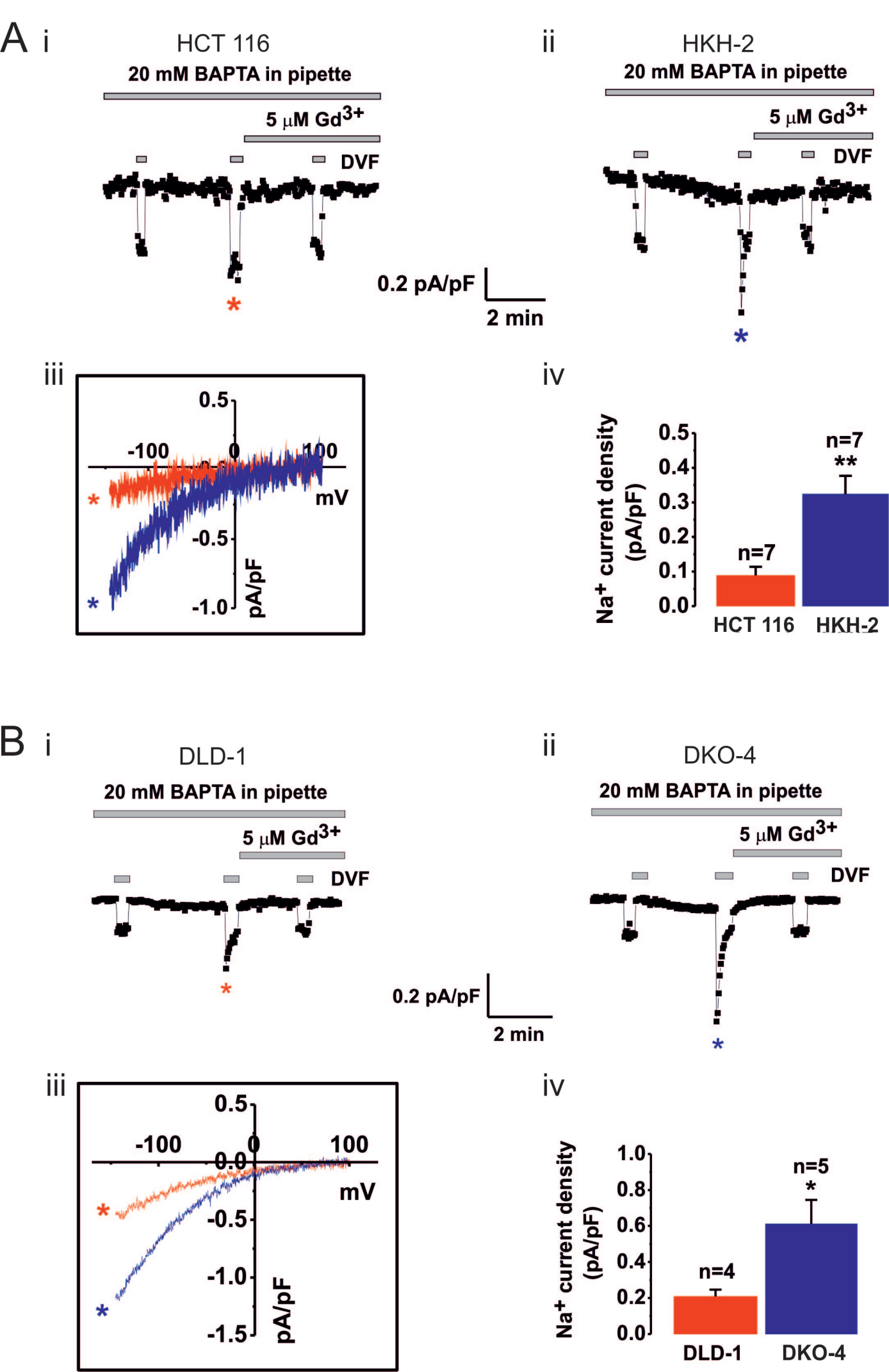
Pipette Solution, pH 7.2: 115 mM Cs-methanesulfonate, 10 mM Cs-1,2-bis-(2-aminophenoxy)ethane-N,N,N′,N′-tetraacetic acid (Cs-BAPTA), 5 mM$CaCl_2$, 8 mM $MgCl_2$, and 10 mM HEPES (pH adjusted with CsOH).

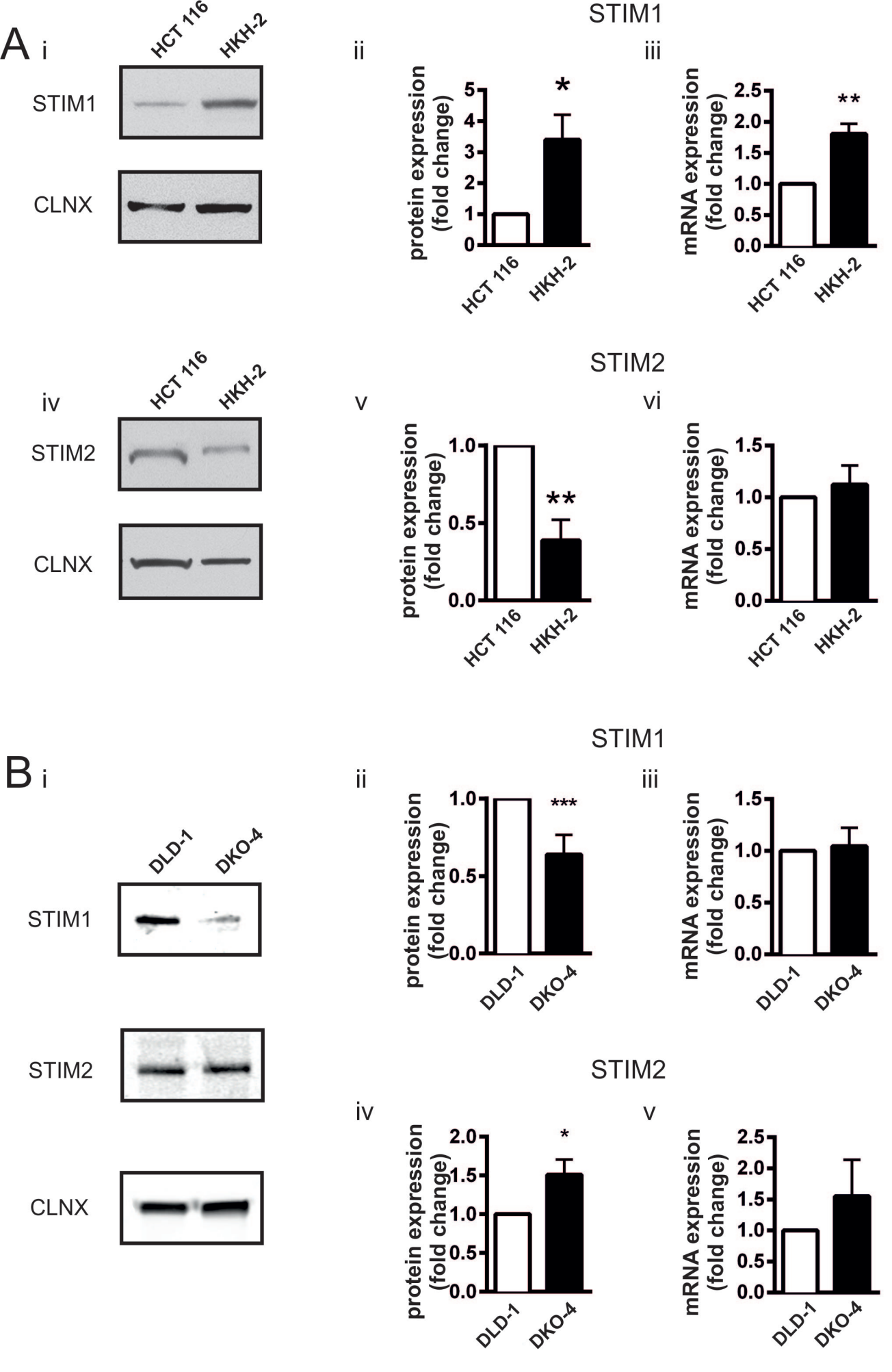
Divalent-free (DVF) bath solution, pH 7.4: 155 mM Na-methanesulfonate, 10 mM HEDTA, 1 mM EDTA, and 10 mM HEPES (pH adjusted with NaOH).

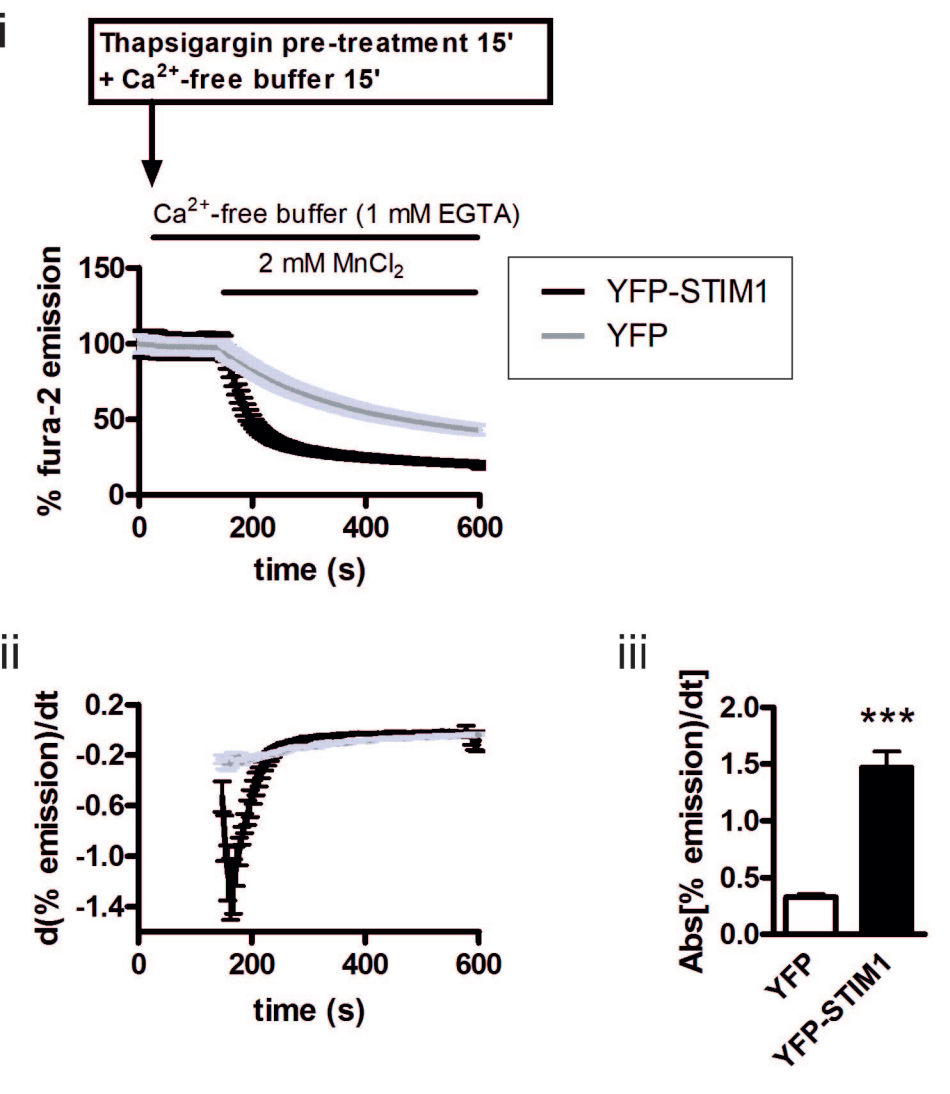
Primer Sequences:

PABPC1	Forward	CTACCAGCCAGCACCTCCTT
	Reverse	CGAGGACTTGGTCTTAGTTGAGC
ELL2	Forward	ACGGTCATTGGAGTCAGTGCT
	Reverse	CAGCGTCTCTACTAGAACATACAGGAG
GAPDH	Forward	GAGTCAACGGATTTGGTCGT
	Reverse	GACAAGCTTCCCGTTCTCAG
STIM1	Forward	TGAAGGCTCTGGATACAGTGCTC
	Reverse	CACCAATAACGATAGACACCACCA
STIM2	Forward	AATTGCTGGAGGAGTTGATGACTT
	Reverse	AGGCTGCTGCTTCTGGCTAA


A
i
Ca2+-free buffer
Ca2+-containing buffer
[Ca2+] (nM)
time (s)
TG
ii
normalised Ca2+ signal
time (s)
HCT 116
HKH-2
iii
d(%Ca2+)/dt
time (s)
iv
d(%Ca2+)/dt
***
HCT 116
HKH-2
B
i
Ca2+-free buffer 15' +
15' Thapsigargin pre-treatment
Ca2+-free buffer (1 mM EGTA)
2 mM MnCl2
% Fura-2 emission
time (s)
HCT 116
HKH-2
ii
d(% emission)/dt
time (s)
iii
Abs[d(% emission)/dt]
***
HCT 116
HKH-2


A
i
HCT 116
20 mM BAPTA in pipette
5 μM Gd3+
DVF
0.2 pA/pF
2 min
ii
HKH-2
20 mM BAPTA in pipette
5 μM Gd3+
DVF
iii
0.5
-100
0
100
mV
-0.5
-1.0
pA/pF
iv
Na+ current density (pA/pF)
0.5
0.4
0.3
0.2
0.1
0.0
n=7
**
n=7
HCT 116
HKH-2
B
i
DLD-1
20 mM BAPTA in pipette
5 μM Gd3+
DVF
0.2 pA/pF
2 min
ii
DKO-4
20 mM BAPTA in pipette
5 μM Gd3+
DVF
iii
0.5
-100
0
100
0.0
mV
-0.5
-1.0
-1.5
pA/pF
iv
Na+ current density (pA/pF)
1.0
0.8
0.6
0.4
0.2
0.0
n=5
*
n=4
DLD-1
DKO-4


A
i
HCT 116
HKH-2
STIM1
CLNX
ii
STIM1
protein expression (fold change)
*
HCT 116
HKH-2
iii
mRNA expression (fold change)
**
HCT 116
HKH-2
iv
HCT 116
HKH-2
STIM2
CLNX
v
STIM2
protein expression (fold change)
**
HCT 116
HKH-2
vi
mRNA expression (fold change)
HCT 116
HKH-2
B
i
DLD-1
DKO-4
STIM1
STIM2
CLNX
ii
STIM1
protein expression (fold change)
***
DLD-1
DKO-4
iii
mRNA expression (fold change)
DLD-1
DKO-4
iv
STIM2
protein expression (fold change)
*
DLD-1
DKO-4
v
mRNA expression (fold change)
DLD-1
DKO-4


i
Thapsigargin pre-treatment 15'
+ Ca2+-free buffer 15'
Ca2+-free buffer (1 mM EGTA)
2 mM MnCl2
YFP-STIM1
YFP
% fura-2 emission
150
100
50
0
0
200
400
600
time (s)
ii
d(% emission)/dt
0.2
-0.2
-0.6
-1.0
-1.4
0
200
400
600
time (s)
iii
Abs[% emission)/dt]
2.0
1.5
1.0
0.5
0.0
***
YFP
YFP-STIM1

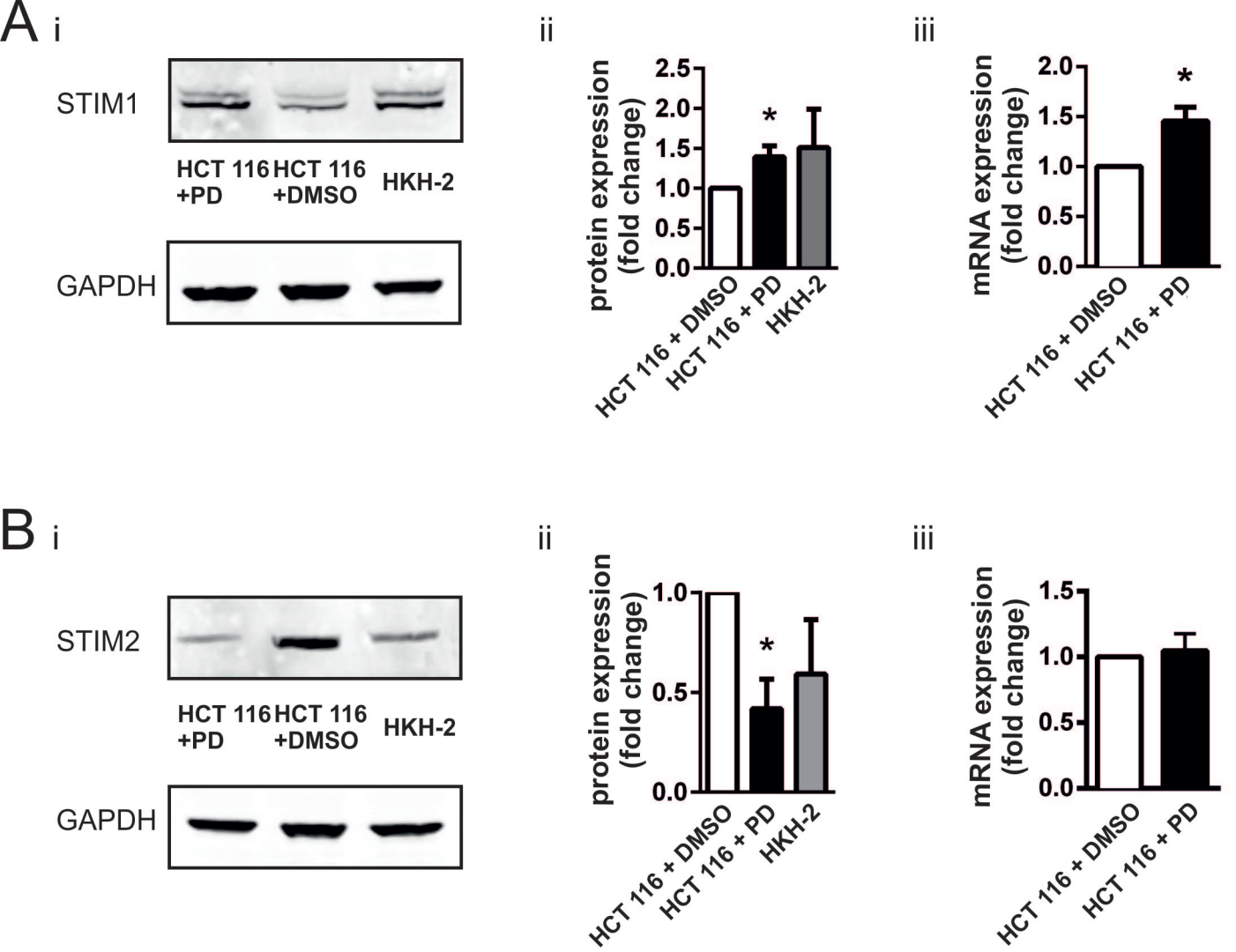

A
i
STIM1
HCT 116 +PD
HCT 116 +DMSO
HKH-2
GAPDH
ii
protein expression (fold change)
2.5
2.0
1.5
1.0
0.5
0.0
*
HCT 116 + DMSO
HCT 116 + PD
HKH-2
iii
mRNA expression (fold change)
2.0
1.5
1.0
0.5
0.0
*
HCT 116 + DMSO
HCT 116 + PD
B
i
STIM2
HCT 116 +PD
HCT 116 +DMSO
HKH-2
GAPDH
ii
protein expression (fold change)
1.0
0.5
0.0
*
HCT 116 + DMSO
HCT 116 + PD
HKH-2
iii
mRNA expression (fold change)
1.5
1.0
0.5
0.0
HCT 116 + DMSO
HCT 116 + PD

Fig.1 SOCE is greater in KRAS^{G13D} null HKH-2 cells than in KRAS^{G13D}-expressing HCT 116 cells. A: i. Overview of the imaging protocol used to assess SOCE. ER Ca^{2+} stores were depleted by Tg application in Ca^{2+}-free buffer, after which Ca^{2+}-containing buffer was superfused over the cells to induce SOCE. **ii.** SOCE response normalised to the peak $[Ca^{2+}]_i$ level. **iii.** Traces of the first derivative of the normalised data from ii. plotted over the time course of the experiment. **iv.** Histogram showing the maximum first derivative of the SOCE signals for HCT 116 and HKH-2 cells. The data represent the mean ± SEM, obtained from four days of experiments, where three coverslips bearing either HCT 116 or HKH-2 cells were imaged on each day. The fields of view chosen for imaging contained at least 60 HCT 116 or HKH-2 cells. *** indicates P < 0.001 (Student's *t*-test). **B: i.** Normalised traces of Mn^{2+} quench of fura-2 fluorescence during excitation at 360 nm in Tg-treated HCT 116 and HKH-2 cells. **ii.** First derivative of the normalised Mn^{2+} quench in i. **iii.** Histogram showing summary data of the maximum first derivative of the Mn^{2+} quench. The data represent the mean ± SEM, obtained from three days of experiments, where three coverslips bearing either HCT 116 or HKH-2 cells were imaged on each day. The fields of view chosen for imaging contained at least 100 HCT 116 or HKH-2 cells. *** indicates P < 0.001 (Student's *t*-test).

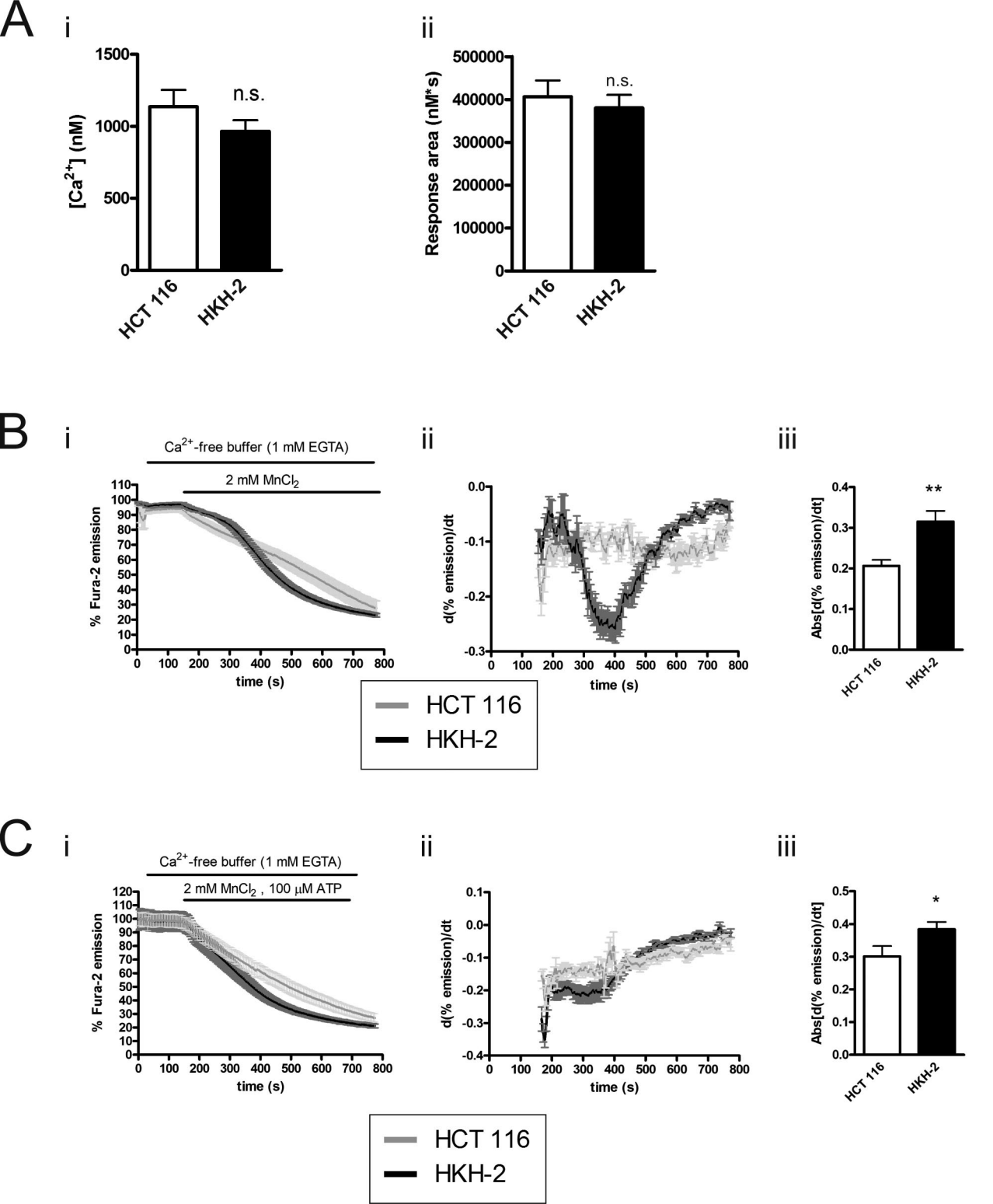
Fig.2. CRAC currents are increased following *KRAS*^{G13D} ablation in the HCT116/HKH2 and DLD-1/DKO4 cell line pairs. Ai-ii and **Bi-ii**. Whole cell CRAC currents activated by 20 mM BAPTA dialysed via patch pipette were measured in extra cellular solution containing 20 mM Ca^{2+}. Na^+ CRAC currents were recorded in divalent free (DVF) solution. Current density recordings over time (pA/pF vs t) in HCT 116 (i) and HKH-2 cells (ii) and in DLD-1 (Bi) and DKO-4 (Bii) cells were taken at -100 mV. Na^+ CRAC during 3 pulses of DVF solution are shown. The first pulse was applied at break-in to gauge leak current, the second pulse was applied when current was maximal, and the third pulse was applied after current inhibition with 5 µM Gd^{3+}. Note rapid depotentiation of CRAC current during the second DVF pulse, a defining characteristic of I_{CRAC}. **Aiii** and **Biii**. I/V relationships of Na^+ CRAC in the HCT 116/HKH-2 and DLD-1/DKO-4 cell line pairs respectively. **Aiv** and **Biv.** Summary data of Na^+ CRAC currents taken at -100 mV in the HCT 116/HKH-2 and DLD-1/DKO-4 cell line pairs respectively. The mean ± SEM and the number of cells are shown (n). * indicates P<0.05 and **P<0.01 determined by Student's *t*-test.

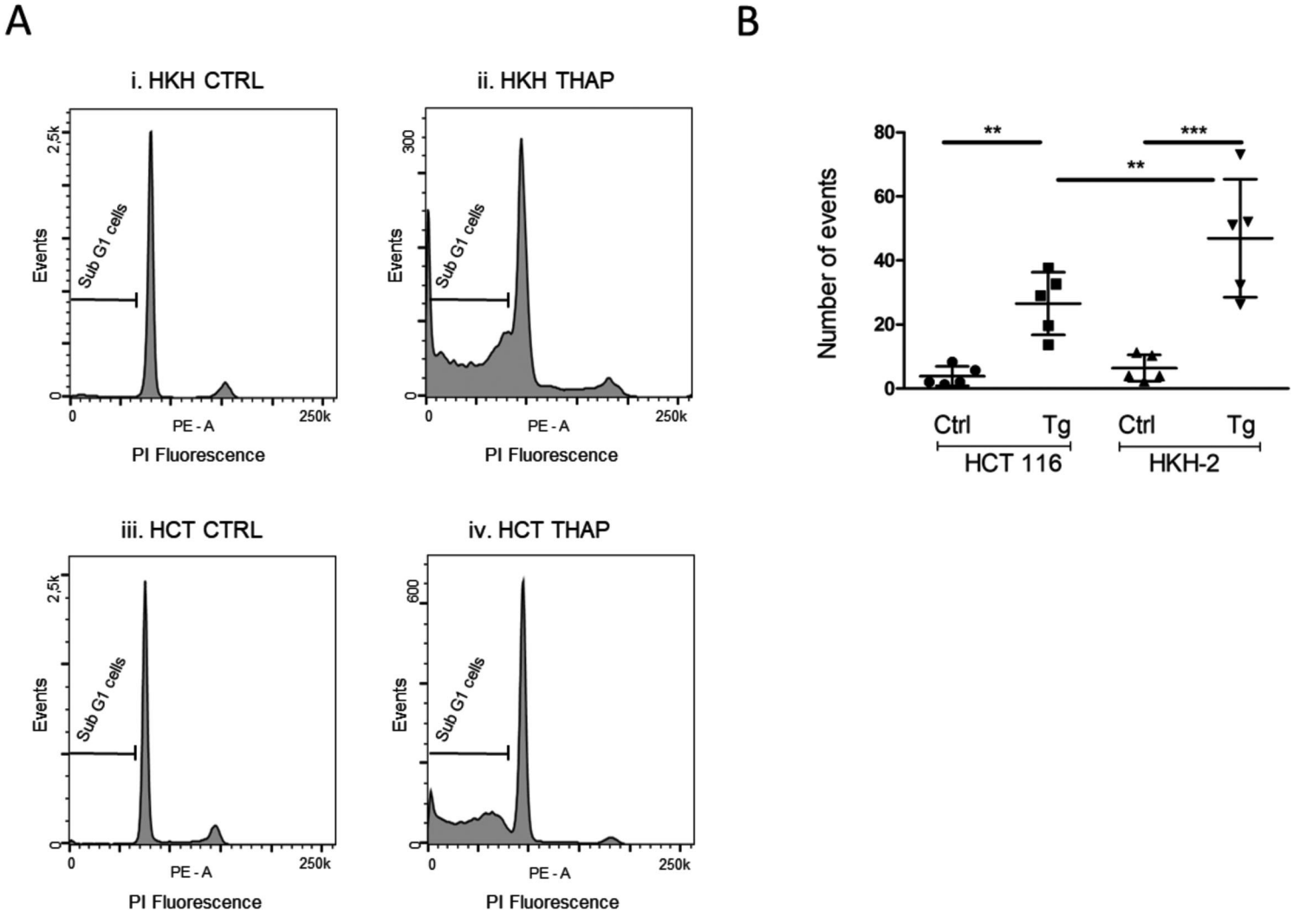
Fig.3. Expression of STIM1 and STIM2 in isogenic CRC cell lines. A. Analysis of STIM1 and STIM2 expression in the HCT 116/HKH 2 cell line pair. **i.** Representative immunoblot of STIM1 in HCT 116 and HKH-2 cells. Calnexin was used a loading control. **ii.** Fold change in STIM1 protein levels in HKH-2 cells with respect to HCT 116 cells. **iii.** Fold change of *STIM1* mRNA expression in HKH-2 cells with respect to HCT 116 determined by RT-qPCR. **iv.** Representative immunoblot of STIM2 in HCT 116 and HKH-2 cells. Calnexin was used a loading control. **v.** Fold change in STIM2 protein level in HKH-2 cells with respect to HCT 116 cells. **vi.** Fold change in *STIM2* mRNA expression in HKH-2 cells with respect to HCT 116 determined by RT-qPCR. **B.** Analysis of STIM1 and STIM2 expression in the DLD-1/DKO-4 cell line pair. **i.** Representative immunoblot of STIM1 in DLD-1 and DKO-4 cells. Calnexin was used a loading control. **ii.** Fold change in STIM1 protein levels in DKO-4 cells with respect to DLD-1 cells. **iii.** Fold change in *STIM1* mRNA expression in DKO-4 cells with respect to DLD-1 measured by RT-qPCR. **iv.** Fold change in STIM2 protein levels in DKO-4 cells with respect to DLD-1 cells. **v.** Fold change in *STIM2* mRNA expression in DKO-4 cells with respect to DLD-1

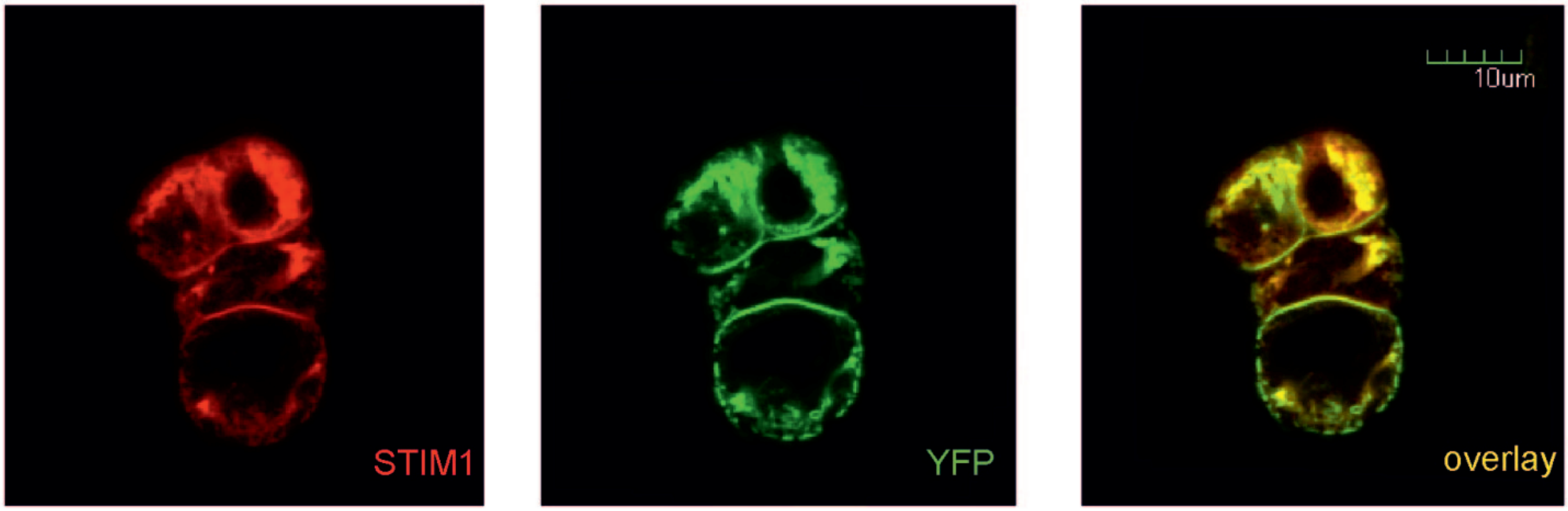
measured by RT-qPCR. All bar graphs represent the mean ± SEM of eight experiments for immunoblotting and six experiments for RT-qPCR. *, ** and *** indicate $P < 0.05$, $P < 0.01$, and $P < 0.001$, respectively (one-sample Student's *t*-test).

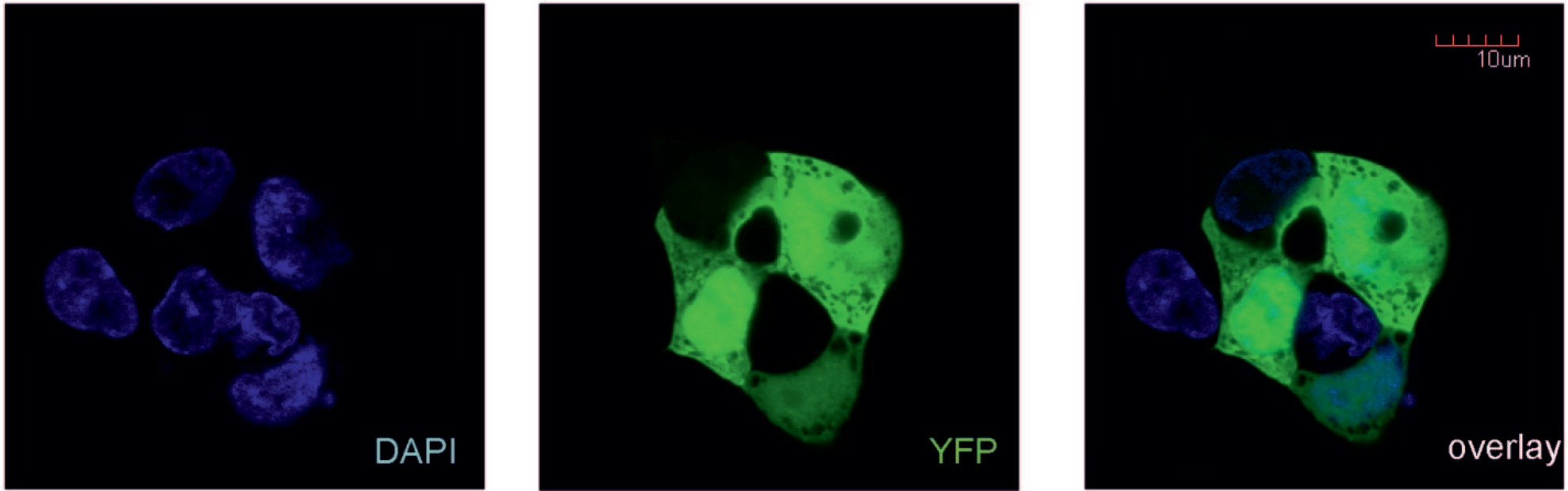
Fig. 4. STIM1 overexpression is sufficient to increase SOCE in HCT 116 cells. i. Normalised fura-2 signal (when excited at 360 nm) in YFP and YFP-STIM1-transfected HCT 116 cells prior and subsequent to addition of $MnCl_2$. **ii.** First derivative of the normalised Mn^{2+} quench of fura-2 fluorescence. **iii.** Summary data showing the maximum value of the derivative of Mn^{2+} quench curve from iii. All graphs represent the mean ± SEM of data from three days of experiments, where 3 coverslips per cell type were imaged on each day. Each coverslip contained at least 30 YFP- or YFP-STIM1-positive cells. *** indicates $P < 0.001$ (Student's *t*-test).

Fig.5. MEK inhibition with PD184352 results in remodelling of STIM1/2 expression in HCT 116 cells. Ai. Representative immunoblot of STIM1 expression in HCT 116 cells treated with PD184352 or DMSO (vehicle control), and of untreated HKH2 cells, as indicated. GAPDH was used as loading control. **ii.** Histogram showing quantification of STIM1 protein expression. **iii.** mRNA levels of *STIM1* in HCT 116 cells treated with DMSO or PD184352 determined by RT-qPCR. **Bi.** Immunoblotting of STIM2 under the same conditions as in Ai. **ii.** Quantification of STIM2 protein expression. **iii.** mRNA levels of *STIM2* following treatment of HCT 116 cells with DMSO or PD184352 determined by RT-qPCR. Histograms of protein expression and for RT-qPCR show a mean ± SEM of 6 experiment each. *represents $P<0.05$ determined by Student's *t*-test.


A
i
[Ca2+] (nM)
1500
1000
500
0
n.s.
HCT 116
HKH-2
ii
Response area (nM*s)
500000
400000
300000
200000
100000
0
n.s.
HCT 116
HKH-2
B
i
Ca2+-free buffer (1 mM EGTA)
2 mM MnCl2
% Fura-2 emission
time (s)
ii
d(% emission)/dt
time (s)
iii
Abs[d(% emission)/dt]
**
HCT 116
HKH-2
HCT 116
HKH-2
C
i
Ca2+-free buffer (1 mM EGTA)
2 mM MnCl2 , 100 μM ATP
% Fura-2 emission
time (s)
ii
d(% emission)/dt
time (s)
iii
Abs[d(% emission)/dt]
*
HCT 116
HKH-2
HCT 116
HKH-2


A
i. HKH CTRL
ii. HKH THAP
iii. HCT CTRL
iv. HCT THAP
Events
Sub G1 cells
PE - A
PI Fluorescence
0
250k
2.5k
300
600
B
Number of events
80
60
40
20
0
**
***
Ctrl
Tg
HCT 116
HKH-2


YFP-STIM1
STIM1
YFP
10um
overlay


YFP
DAPI
YFP
10um
overlay

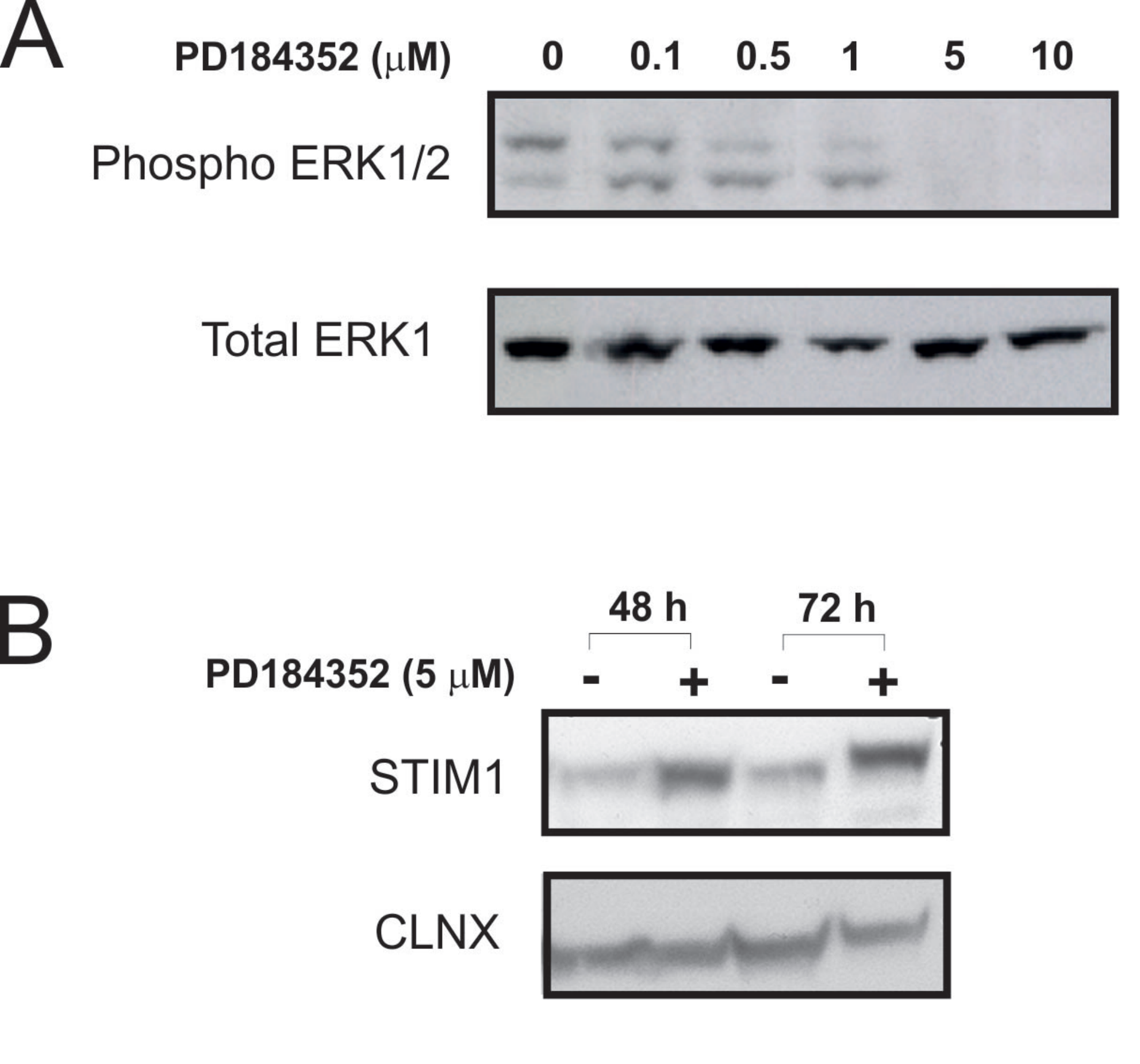

A
PD184352 (μM)
0
0.1
0.5
1
5
10
Phospho ERK1/2
Total ERK1
B
48 h
72 h
PD184352 (5 μM)
-
+
-
+
STIM1
CLNX

Fig. S1. A. Peak amplitude (**i**) and magnitude (**ii**) of SOCE (Ca^{2+} re-addition phase) following Tg-induced Ca^{2+} leak in HCT 116 and HKH-2 cells. **B. i**: Mn^{2+} influx in unstimulated HCT 116 and HKH-2 cells normalised to point of addition revealed by fluorescence quench of fura-2 (excitation at 360 nm). **ii**: first derivative of the normalised Mn^{2+} quench. **iii**: summary data of maximum absolute derivative obtained from the data shown in the centre panel. **C. i**: Mn^{2+} influx in ATP-stimulated HCT 116 and HKH-2 cells normalised to point of addition revealed by quench of fura-2 fluorescence (excitation at 360 nm). **ii**: first derivative of the normalised Mn^{2+} quench. **iii**: summary data of maximum absolute derivative obtained from the data shown in the centre panel. All graphs represent the mean ± SEM of three days of experiments, where 3 coverslips per cell type were imaged on each day. Each coverslip contained at least 100 cells. ** and *** indicate $P < 0.01$ and $P < 0.001$ (Student's *t*-test).

Fig. S2. Analysis of sub G-1 DNA content of HCT 116 and HKH-2 cells following treatment with Tg for 24 h. A. Frequency histograms of PI-stained control and Tg-treated HCT 116 and HKH 2 cells. The x axis indicates intensity of PI staining (DNA content) and the y axis, the number of events (cells). Cells with Sub-G1 DNA content are indicated. **B.** Histogram showing summary data of % of cells with sub-G1 DNA content. The experiment was performed on 6 occasions in triplicate. Statistical significance was determined by 2 way ANOVA and post-hoc test and accepted when $p<0.05$.

Fig. S3. Confocal images of HCT 116 cells transfected with YFP or YFP-STIM1 plasmids. HCT 116 cells transfected with YFP or YFP-STIM1 plasmids were visualised using confocal imaging. Cells were labelled with a primary antibody directed against STIM1, and detected with an ALEXA 568-coupled secondary antibody. YFP and YFP-STIM1 were detected based on the fluorescence of YFP. Nuclei are stained in blue with DAPI. Confocal images of HCT 116 cells transfected with YFP-STIM1 (top row) or with YFP alone (bottom row) are shown. Scale bar = 10 µm.

Fig. S4. Concentration and time dependence of MEK inhibitor PD184352 treatment on ERK1/2 activation (Phospho-ERK) and STIM1 expression in HCT 116 cells. A. Effect of 0 to 10 µM PD184352 for 24 h on ERK1/2 phosphorylation. 5 µM PD184352 was sufficient to suppress MEK, preventing ERK1/2 phosphorylation. Total ERK1 is used as loading control. **B.** Effect of exposure of HCT 116 cells to PD184352 (5 µM) for 48 and 72 h on STIM1 expression. A 48 h treatment was sufficient to cause an increase in STIM1 expression. Blots are representative of three experiments.